

Improving Land Use Change Tracking in the UK  
Greenhouse Gas Inventory. Report on final  
outputs November 2021

Peter Levy, Sam Tomlinson, and Beth Raine

2021-11-10



# Contents

<b>Summary</b>	<b>5</b>
<b>1 Introduction</b>	<b>7</b>
1.1 Tracking land-use change . . . . .	8
1.2 Approach . . . . .	9
<b>2 Quantifying Uncertainty in Land-Use Data Sources</b>	<b>11</b>
2.1 Introduction . . . . .	11
2.2 Representation of uncertainty . . . . .	12
2.3 Defining reference data . . . . .	13
2.4 Options for improvement . . . . .	13
2.5 Producing uncertainty estimates . . . . .	14
2.6 Conclusions . . . . .	21
<b>3 Assessing systematic errors in estimates of land-use change: sensitivity to survey-interval length</b>	<b>23</b>
3.1 Introduction . . . . .	23
3.2 Methods . . . . .	24
3.3 Results . . . . .	25
3.4 Discussion and Conclusions . . . . .	31
<b>4 Estimating false-positive rates in detection of land-use change based on classification accuracy</b>	<b>33</b>
4.1 Introduction . . . . .	33
4.2 Methods . . . . .	33
4.3 Results . . . . .	34
4.4 Conclusions . . . . .	36
<b>5 Using life tables in modelling land-use change</b>	<b>39</b>
5.1 Introduction . . . . .	39
5.2 Illustration with dummy data . . . . .	40
5.3 Next steps . . . . .	41
<b>6 Results: England</b>	<b>43</b>

<b>7 Results: Scotland</b>	<b>53</b>
<b>8 Results: Wales</b>	<b>63</b>
<b>9 Results: Northern Ireland</b>	<b>73</b>

# Summary

This report describes work on the project “Improving Land Use Change Tracking in the UK Greenhouse Gas Inventory” for the Department for Business, Energy & Industrial Strategy (reference TRN 2384/05/2020). The aim of the project was to make improved estimates of land-use change in the UK, using multiple sources of data. We applied a method for estimating land-use change using a Bayesian data assimilation approach. This allows us to constrain estimates of gross land-use change with national-scale census data, whilst retaining the detailed information available from several other sources. We produced a time series of maps describing our best estimate of land-use change given the available data, as well as the full posterior distribution of this space-time data cube. This quantifies the joint probability distribution of the parameters, and properly propagates the uncertainty from input data to final output. The output data has been summarised in the form of land-use vectors. The results show that we can provide improved estimates of past land-use change using this method. The main advantage of the approach is that it provides a coherent, generalised framework for combining multiple disparate sources of data, and adding further sources of data in future would be straightforward. Future work could focus on more detailed analysis of existing data sets, introducing independent constraints where possible, and obtaining further relevant data sets. The code is available via GitHub.



# Chapter 1

## Introduction

This report describes work carried out on the project “Improving Land Use Change Tracking in the UK Greenhouse Gas Inventory” for the Department for Business, Energy & Industrial Strategy (reference TRN 2384/05/2020). The aim of the project was to make improved estimates of land-use change in the UK, using multiple sources of data, using a Bayesian data assimilation approach. Two previous reports describe the background to the project and results from Work Package (WP) A (Levy et al. 2020), using pre-existing data sets, and work developing new data sets based on Earth Observation in WP-B (Rowland et al. 2021). This report describes subsequent work which focussed on assessing the uncertainties in data sets, and incorporating these in the data assimilation procedure. Specifically, we aimed to:

- quantify random uncertainty in the different data sources;
- quantify systematic uncertainty, i.e. biases which may make a data source under- or over-estimate land-use change;
- represent the uncertainty associated with the different sampling frequencies of the data sources (e.g. annual versus decadal surveys);
- handling the uncertainty associated with the different temporal coverage of the data sources (avoiding step changes when data coverage starts or stops);
- incorporate some additional data sets which were not previously available because of data access or processing time constraints;
- improve the representation of the rotational change between crop and grassland.

The above were incorporated in the data assimilation procedure, and results produced for each of the Devolved Administrations (DAs) of the UK. Land-use change on mineral soil and organic soil was estimated separately in each DA.

The remainder of this report describes these tasks and the resulting estimates of land-use change produced after their inclusion.

The first section on quantifying uncertainty describes how uncertainty is represented, and estimates random and systematic uncertainty by comparison with a reference data set.

The next section describes an alternative method for systematic uncertainty based on the length of the interval between surveys. As a third method, we then look at how errors in map classification propagate into errors in estimates of land-use change.

Next, we describe a method for more accurately representing the frequency of rotational land-use change, using the idea of “life tables” borrowed from population modelling.

The previous reports give detailed descriptions of the methods. However, here we reproduce the basic rationale and approach of the project for background.

## 1.1 Tracking land-use change

The tracking of land use and land-use change is fundamental to producing accurate and consistent greenhouse gas inventories (GHGI) for the Land Use, Land-Use Change and Forestry (LULUCF) sector. This is necessary to meet the international requirements of the Kyoto Protocol to the UN Framework Convention on Climate Change (UNFCCC) and the Paris Agreement and the national requirements of the UK’s Climate Change Act and related legislation within the UK’s Devolved Administrations.

The estimation of land-use change in the current UK GHGI is based on a combination of infrequent CEH Countryside Surveys and afforestation/deforestation statistics from the GB Forestry Commission. It uses Approach 2 (non-spatial land-use change matrices) as described in the KP Guidance. However, this matrix-based approach, and its implementation in the UK, have some important limitations. Firstly, the non-spatial matrix-based approach is insufficient for tracking annual land-use change: the matrices have no time dimension, and are defined independently each year. There is therefore no possibility of representing a sequence of land-use on the same parcel of land (such as afforestation followed by deforestation, or crop-pasture rotations). Secondly, the data used to estimate these matrices in the UK are rather limited. The CEH Countryside Surveys were only carried out approximately once per decade, and whilst the geographical extent was very wide, the actual ground area surveyed was small as a fraction of the total UK area. The afforestation/deforestation statistics from the Forestry Commission have good national coverage (excluding Northern Ireland) but do not contain any information on the spatial location or land use prior to afforestation or following deforestation.

In October 2019, the UNFCCC Expert Review of the UK 1990-2017 GHG inventory raised concerns in relation to the reporting requirements of the second commitment period of the Kyoto protocol. They questioned whether the current

approach is appropriate for the identification and tracking of lands where the elected Article 3.4 activities occur (i.e. Cropland Management, Grazing Land Management and Wetland Drainage and Rewetting). They recommended that the UK explore how to make the best possible use of available data and prepare and implement a work-plan to enable the use of these data. The UK has already explored several approaches to land use tracking, including a data assimilation approach to integrate available land-use data into land-use vectors, which was successfully piloted in Scotland (Levy et al. 2018). This project builds on that approach to assess gross land-use change, and land-use history for the whole of the UK from 1990 to 2019.

As well as improving accuracy of the GHGI, a time series of spatially explicit land-use change would enable better tracking of mitigation activities and improve baseline data for scenario modelling. These baseline data are needed for understanding the potential of land-based mitigation and adaptation options. The government's ambitions for Net Zero by 2050 or sooner means that the LULUCF sector will have an increasingly critical role in the UK's overall GHG balance. This kind of scenario modelling will become very important to inform the setting of future carbon budgets and monitor progress towards the UK's legal obligations to GHG emissions reductions. An accurate spatio-temporal land-use change data set would be useful to other stakeholders and UK government departments. For example, from the perspectives of biodiversity conservation, air quality, or ecosystem services, there are clear applications of these data for understanding and tracking the effects of land use.

## 1.2 Approach

If we had reliable maps of land use each year, we could infer land-use change by difference. However, even with advances in satellite sensors, GIS and spatial data handling, the accuracy of change detection from EO-based products is generally too poor to do this; the different EO products are inconsistent (with each other, and with themselves over time), irregular, and become more infrequent as we go back in time. Change is more reliably detected by repeat ground-based surveys, but these have other short-comings. For example, the annual June Agricultural Census gives a long record of areas in different land uses, but does not provide spatial data, or any information on gross change (i.e. what land uses have changed to which other land uses). The CEH Countryside Survey did provide spatial data with gross change, but without complete coverage, and only at infrequent intervals.

In light of the above, some data assimilation method, which combines the spatio-temporal data with non-spatial repeat survey data, would appear to provide a solution. To this end, we previously developed a methodology using a Bayesian data assimilation approach, and this has been applied successfully to Scotland (Levy et al. 2018). This method allowed for the use of a wider range of data types, including high-resolution spatial data, and combined them in a mathematically

coherent way. Importantly, the method produced the appropriate data structure needed for modelling the effects of land-use change on GHG emissions - the set of unique land-use vectors (i.e. unique sequences of land use, or land-use histories) and their associated areas. An important feature is that the uncertainty in land-use change can be easily propagated to provide the uncertainty in GHG emissions, because the procedure explicitly handles the distribution of plausible vectors of land-use change. The approach provides a general framework for combining multiple disparate data sources with a simple model which describes how these data sources inter-relate. This allows us to constrain estimates of gross land-use change with reliable national-scale census data, whilst retaining the detailed spatial information available from several other sources. Here, we apply this methodology to improve and update the tracking of land-use change for the UK. Our aim was to apply a Bayesian approach to make spatially- and temporally-explicit estimates of land-use change in the UK, using multiple sources of data.

All the code is written in R using the “literate programming” paradigm implemented with Rmarkdown, which combines the source code, text/graphical output, documentation, and report text within the same document. This ensures integrity of documentation, code and corresponding outputs. All the Rmarkdown files are held in a GitHub repository, for version control and wider accessibility. The documentation is rendered using bookdown and made publicly available as a web site via GitHub Pages. This documentation describes the data processing workflow so as to make it reproducible.

## Chapter 2

# Quantifying Uncertainty in Land-Use Data Sources

### 2.1 Introduction

Several different data sources provide observations of the transition matrix  $B$ , as well as net and gross change in area of each land use ( $D, G, L$ ). The method used in WP-A treated all data sources as equally uncertain, and assumed the same relative error for all observations. However, in reality, we know that these data sets have different levels of uncertainty: some data sets are closer to direct observations, are more plausible, and we have greater faith in these. We want to reflect this in the methodology by quantitatively associating different uncertainties with each data set. This is straightforward in principle, but there are several considerations when doing this in practice:

1. We can consider increasing levels of detail:
  - variable-specific uncertainties (i.e. different for  $B, G, L$  &  $D$ )
  - data source type-specific uncertainties (i.e. different for ground-based vs EO data)
  - data set-specific uncertainties (i.e. different for CS, IACS, LCM etc.)
  - land-use type-specific uncertainties (i.e. different for woods, crops, grass etc.)
  - time-specific uncertainties (i.e. different for 1990, 2000 ... 2019)
2. Rather than continuous data with a simple  $\sigma$  error term, the  $B$  observations are count data in a  $6 \times 6$ -way classification. When considering land-use *change*, we need to compare the 36 elements of this classification from one data source with another (or the truth), so we have a  $36 \times 36$  error

matrix (or “confusion” matrix). This matrix has two distinct types of errors that we ideally want to distinguish: false positives and false negatives, or “user”/“commission” and “producer”/“omission” error/accuracy, in the terminology commonly used in remote sensing.

3. We can specify uncertainty greater or lesser rigour: there are several possibilities for how we represent “uncertainty” in the mathematical model.
4. We can estimate uncertainty subjectively, or base it more closely on data. There are also several possibilities for how we translate measures of uncertainty in the data in to the mathematical model.

A limitation is that none of the data sources represents absolute truth, and we have no clear reference data set against which to calibrate.

## 2.2 Representation of uncertainty

The data sources are assimilated in the Bayesian method in the likelihood function, which includes a term  $\sigma^{obs}$ , representing the standard deviation in the probability density function for the observation. The observation is thus not assumed to be the true value, but subject to errors which make it deviate from this. Uncertainty is thus represented by the magnitude of  $\sigma^{obs}$  - large values of  $\sigma^{obs}$  represent high uncertainty. For each observation, a likelihood is calculated, assuming that measurement errors show a Gaussian distribution and are independent of each other. In mathematical notation, the likelihood of observing the area changing from land use  $i$  to land use  $j$ ,  $\beta_{ij}^{obs}$ , is

$$\mathcal{L} = \frac{1}{\sigma_{ij}^{obs}\sqrt{2\pi}} \exp(-(\beta_{ij}^{obs} - \beta_{ij}^{\text{pred}})^2 / 2\sigma_{ij}^{obs^2}) \quad (2.1)$$

where  $\beta_{ij}^{\text{pred}}$  is the corresponding prediction, and  $\sigma_{ij}^{obs}$  is the uncertainty in the observation. There are analogous terms for  $G$ ,  $L$  and  $D$  which can all be multiplied. For example, the term for the likelihood of observing the net change in land use  $u$ ,  $D_u^{obs}$ , is

$$\mathcal{L} = \frac{1}{\sigma_u^{obs}\sqrt{2\pi}} \exp(-(D_u^{obs} - D_u^{\text{pred}})^2 / 2\sigma_u^{obs^2}) \quad (2.2)$$

We previously assumed that *relative* measurement uncertainty was the same for all observations, i.e. a constant proportion of the observed value. Thus, observations of large areas come with larger absolute uncertainty. The question is how to estimate more specific uncertainties  $\sigma^{obs}$  for the different data sources, if not specific for each individual observation. We thus need to examine the basis for specifying these uncertainties, based on a proper quantitative analysis.

## 2.3 Defining reference data

A pre-cursor step is to define a reference data set with which we compare each data source, in the absence of ideal ground-truth data. We could decide on a reference data set which we believe to be the most plausible or closest to the truth, based on judgement and prior knowledge. Some subjectivity is inevitable here, and would need to be justified and explicit. An alternative would be a version of the “leave-one-out” cross-validation idea: each data source is tested against all the other remaining data sources. With some subjective weighting applied to the data sources, the two ideas could be combined.

## 2.4 Options for improvement

We consider here some options for improving the representation of data set-specific uncertainty in the methodology. These are in increasing order of complexity, and are not mutually exclusive.

1. Most simply, we could base all  $\sigma^{\text{obs}}$  on the “lowest common denominator” data set, the time series of net area change  $D$ . Irrespective of higher levels of detail, all data sources produce estimates of  $D$ . If we define a reference data set, we can calculate a metric of agreement with this for all other data sets. Suitable metrics would be root-mean-square error (RMSE), mean-absolute error (MAE) and/or the correlation coefficient. We can use this metric as a scaling factor in estimating  $\sigma^{\text{obs}}$ , such that data sources with poor agreement receive high  $\sigma^{\text{obs}}$  (high uncertainty). Some subjectivity would come into deciding on the reference data set, which metrics to use, and the absolute values of  $\sigma^{\text{obs}}$ , but the relative uncertainties (and therefore weighting) would be based quantitatively on data. Extending this approach to  $G$  and  $L$  data would be straightforward.
2. Similarly, but focussing on the  $B$  data, if we define a reference data set, we can calculate confusion matrices. We can then calculate metrics of overall agreement, and there are many such metrics - accuracy, precision, prevalence, misclassification rate, etc. There is much debate about these metrics, but a reasonable choice in our case would be the  $\kappa$  statistic:

$$\kappa = 1 - \frac{1 - p_o}{1 - p_e} \quad (2.3)$$

where  $p_o$  is the relative observed agreement with the reference data (the number of grid cells correctly classified), and  $p_e$  is the hypothetical probability of chance agreement (calculated from the products of the confusion matrix row sums and columns sums). With perfect agreement,  $\kappa = 1$ ; with no agreement beyond what would be expected by chance,  $\kappa = 0$ . This gives a more robust measure than simple percentage agreement, with a convenient scaling.  $\kappa$  does not translate into an exact value for  $\sigma^{\text{obs}}$ , but is clearly related. We can therefore use  $\kappa$  as a scaling factor in estimating

$\sigma^{\text{obs}}$ , such that data sources with low  $\kappa$  values (poor agreement) receive high  $\sigma^{\text{obs}}$  (high uncertainty). The same elements of subjectivity come into this approach, but the quantity of data and level of detail used is greater. If we have the predictive probabilities associated with each prediction, we can plot the “receiver operating characteristics” graph or ROC, and also the Area Under the Curve (AUC). This metric has several theoretical advantages, but is more complex to calculate.

3. A fundamentally different approach is to explicitly represent the false positive and false negative error terms in the likelihood function. False positives cause observations to over-estimate change, whilst false negatives produce an under-estimate. The estimated bias in the observation is a simple function of the false positive and false negative error rates ( $F_P$  and  $F_N$ ) and the area (and number of grid cells) in which the false negative errors can occur,  $A_N$ . The likelihood equation becomes:

$$\mathcal{L} = \frac{1}{\sigma_{ij}^{\text{obs}} \sqrt{2\pi}} \exp(-((1 - F_P)\beta_{ij}^{\text{obs}} + A_N F_N - \beta_{ij}^{\text{pred}})^2 / 2\sigma_{ij}^{\text{obs}})^2) \quad (2.4)$$

This then calculates the likelihood of the observed change from land use  $i$  to land use  $j$ , given that the true value is  $\beta_{ij}^{\text{pred}}$ , and with given false positive and false negative rates  $F_P$  and  $F_N$ , and uncertainty  $\sigma_{ij}^{\text{obs}}$  in the observation. This approach can be implemented in increasingly complex ways:

- estimating the false positive and false negative error rates based on some set of confusion matrices, and thereafter assuming them to be fixed and constant for a given data source;
- as above, but calculating false positive and false negative error rates specific to each type of land-use change (i.e.  $F_{Pij}$  and  $F_{Nij}$ ), and potentially varying in time;
- including the false positive and false negative error rates as unknown parameters to be calibrated, along with the  $B$  and  $\sigma^{\text{obs}}$  values. This is the most sophisticated solution, as it properly represents the fact that these are not truly known, and allows the values to be an emergent property of the data, given prior information, rather than imposing our guesses. The exact number of these parameters to estimate could vary as above, whether specific to each data source, type of land-use change, and point in time.

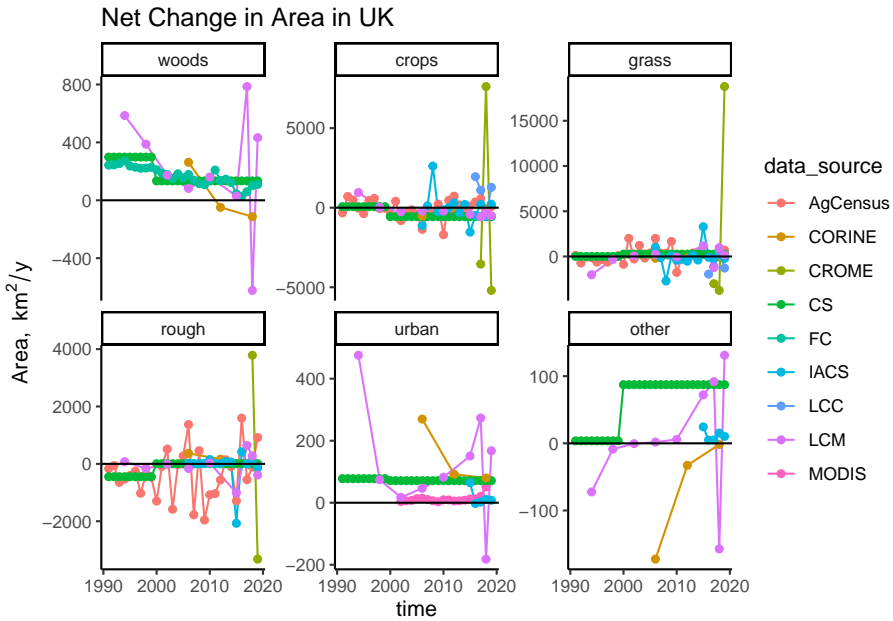
## 2.5 Producing uncertainty estimates

We have explored the use of sigma scaling and using false positive and false negative rates in the datasets at the land-use, data-source and time levels to identify the most appropriate way to account for uncertainty in the data assimilation. The reference raster creation, calculation of false positives and

negatives and application of these values into the likelihood function is presented below.

### 2.5.1 Sigma scaling approach:

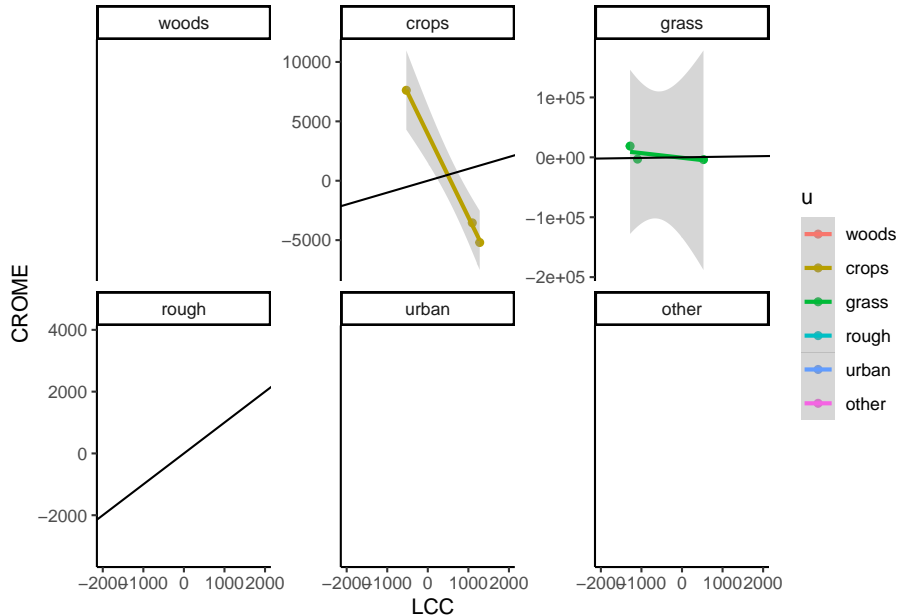
We can apply option 1 in its simplest form by basing the scaling factor for  $\sigma^{\text{obs}}$  on the net area change  $D$ . We define the reference data set as the June Agricultural Census data for crops, grass and rough, and the FC data for forests. The table below shows two metrics, the RMSE and the correlation coefficient. We combine these in a multiplicative way (using  $1/(r^2 + 1)$ ) to give a single scaling factor for  $\sigma^{\text{obs}}$  (“sigma\_scaling” in the table). The ranking shows that IACS has the lowest uncertainty and the Land Cover Crop Maps has the highest (bearing in mind all the imperfections in the reference data). This produces a quantitative means of accounting for the different relative uncertainties in these data sources.



	RMSE	r2	sigma	Fp	Fn
AgCensus	0.00000	1.0000000	4.46397	0	0
FC	0.00000	1.0000000	4.46397	0	0
CORINE	170.53335	0.9476470	8.92794	0	0
CS	58.21941	0.7358905	15.37630	0	0
LCM	378.85076	0.2222080	294.66711	0	0
LCC	NA	NA	NA	0	0
IACS	NA	NA	NA	0	0
CROME	NA	NA	NA	0	0

An example is shown below.

```
## `geom_smooth()` using formula 'y ~ x'
```



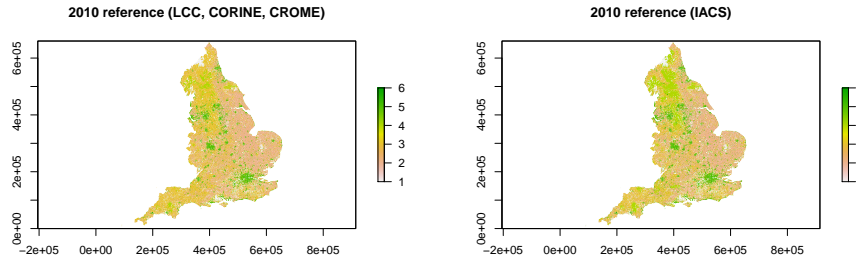
### 2.5.2 False positive and negative approach:

### 2.5.3 Creating reference datasets:

We created the reference data by combining several spatially explicit data sources that are thought to have the highest accuracy and reliability for certain land use types, namely FC, IACS and LCM. These data-sources were added to the reference dataset in order meaning land use defined in FC data took precedent over IACS, followed by LCM. This was considered the most sensible approach to build the dataset based on reliability of land use classes in each dataset meant the overall reference raster would be as reliable as possible and also limit the number of undefined cells. This resulted in a reference dataset that includes the majority of forest cells from FC, the majority of crop, grass and rough grazing from IACS and the majority of urban and other cells from LCM. This reference data was used to compare the other data-sources against (LCC, CORINE, CROME). In order to test FC, IACS and LCM themselves, we removed the respective dataset from the reference data, and tested land use change classifications against those present in the remaining reference data(e.g. testing the forest, crop, grassland or rough grazing land use change in IACS against that defined in FC and LCM).

This method enabled us to build reference rasters for England for 2006, 2010, 2015, 2017, 2018 and 2019, the 2010 reference raster for LCC, CORINE and CROME (including FC, IACS and LCM) is shown below, as well as the 2010 reference raster for testing IACS (including FC and LCM). In the IACS reference

dataset, land use from LCM is used in place of IACS.



The table below shows the reference data contents for each data source:

Dataset	Reference
FC	IACS, LCM
IACS	FC, LCM
LCM	FC, IACS
LCC	FC, IACS, LCM
CORINE	FC, IACS, LCM
CROME	FC, IACS, LCM

#### 2.5.4 Confusion matrices

The reference data is then used to compare land use change between two years in the test data source to what we have assumed as the correct land use change between these years. The 36\*36 confusion matrix produced gives the total change from one land use to another identified in the reference raster as column sums, and the total change from one land use to another identified in the test data as the row sums. The diagonal identifies the area of land use change that was identified to occur in both the reference and test data sets. This is used to calculate the false positive and false negative rates for each land use type.

##### 2.5.4.1 False positive rates

The false positive rate, the rate of incorrectly observing the area changing from land use  $i$  to land use  $j$  in the test dataset compared to the reference dataset, is calculated as:

$$F_{Pij} = (B_{test,ij} - B_{ref,ij}) / B_{test,ij}$$

Where  $B_{test,ij}$  is the total observed area of land changing in the test dataset and  $B_{ref,ij}$  the total area in the reference dataset.

##### 2.5.4.2 False negative rates

The false negative rate, the rate of failing to observe land use change from  $i$  to  $j$  in the test dataset compared to the reference dataset, is calculated as:

$$F_{Nij} = (B_{ref,ij} - B_{ref,test,ij}) / c - B_{test,ij}$$

Where  $B_{ref,test,ij}$  is the total area of land changing from  $i$  to  $j$  identified in both the reference and test dataset and  $c$  is the total area of England, making the denominator the total available land area that could have changed from  $i$  to  $j$  in the test dataset but did not.

Here we use CORINE as an example showing the false positive and negative rates calculated between the data source and the reference dataset between 2006 and 2018 (most recent years available for comparison). The data shows the trend across all of the data-sources: low false negative rates and high false positive rates, with slightly lower false positive rates for the land use change between crop and grassland. The matrices below show the false positive/negative rate for each land use change between the first year (row) and the second year (column).

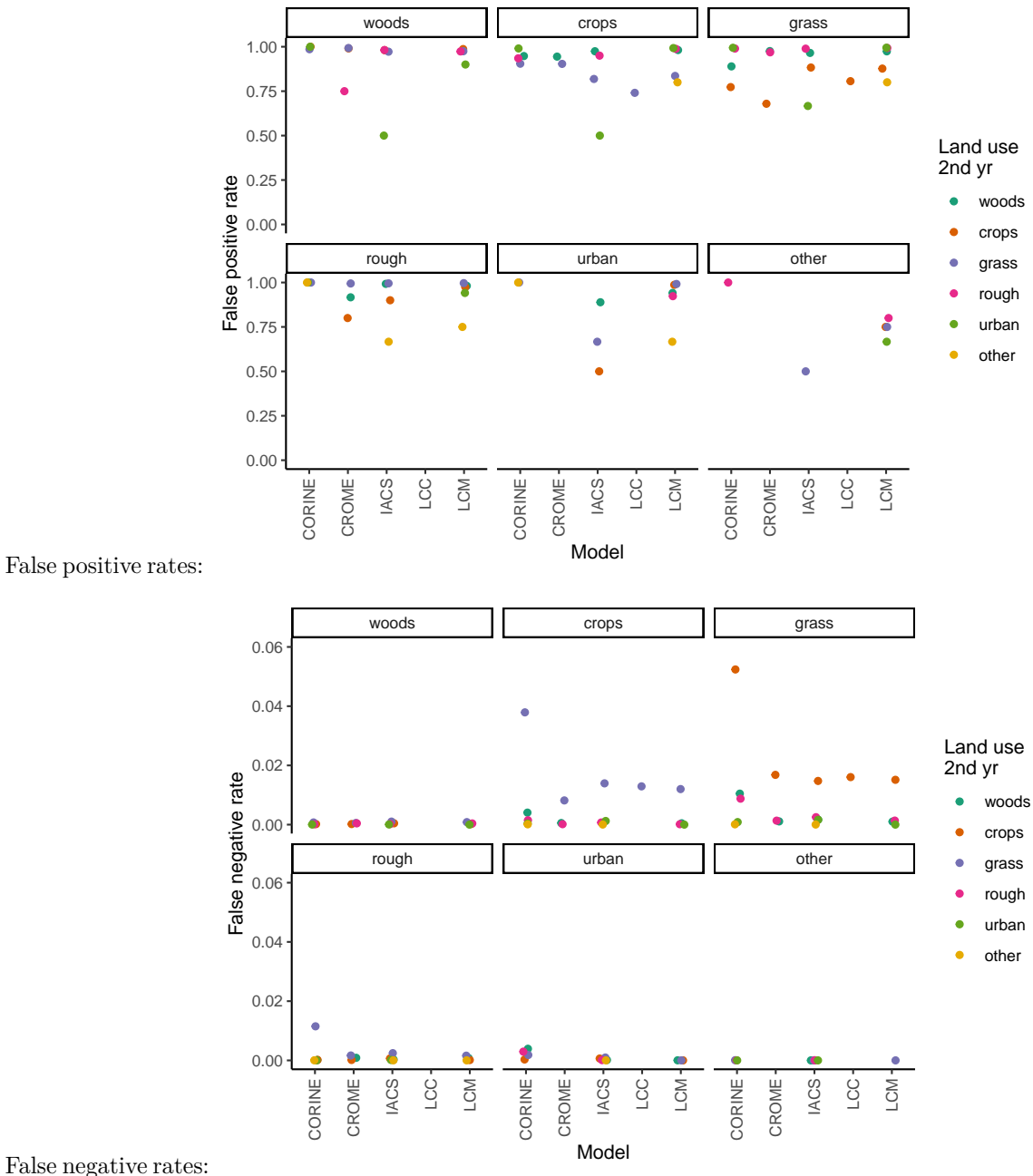
False positive rates for CORINE between 2006 and 2018:

	woods	crops	grass	rough	urban	other
woods		1	0.992	1	1	0
crops	0.977		0.928	0.949	0.994	1
grass	0.951	0.767		0.996	0.991	1
rough	1	1	1		1	1
urban	1	1	0.985	1		1
other	0	1	1	1	0	

False negative rates for CORINE between 2006 and 2018:

	woods	crops	grass	rough	urban	other
woods		0	0.001	0	0	0
crops	0.004		0.038	0.001	0	0
grass	0.01	0.053		0.009	0.001	0
rough	0	0	0.011		0	0
urban	0.004	0	0.002	0.003		0
other	0	0	0	0	0	

The following graphs show the false positive and false negative rates for each data source, with the grid of graphs showing the land use type in the first year and colour showing the land use in the second year.



### 2.5.5 Data-set level false positive and false negative rates

Based on the very high false positive rates identified for many of the land use change classes, we have chosen to implement false positive rates at the data-set

level rather than land-use level. We are not integrating the false negative rate to the likelihood function at this point as they are strongly influenced by the form of the reference dataset and as a result are highly subjective. Data-set level false positive rates were calculated as an average of the land-use level false positive rate, weighted by area of each land-use change.

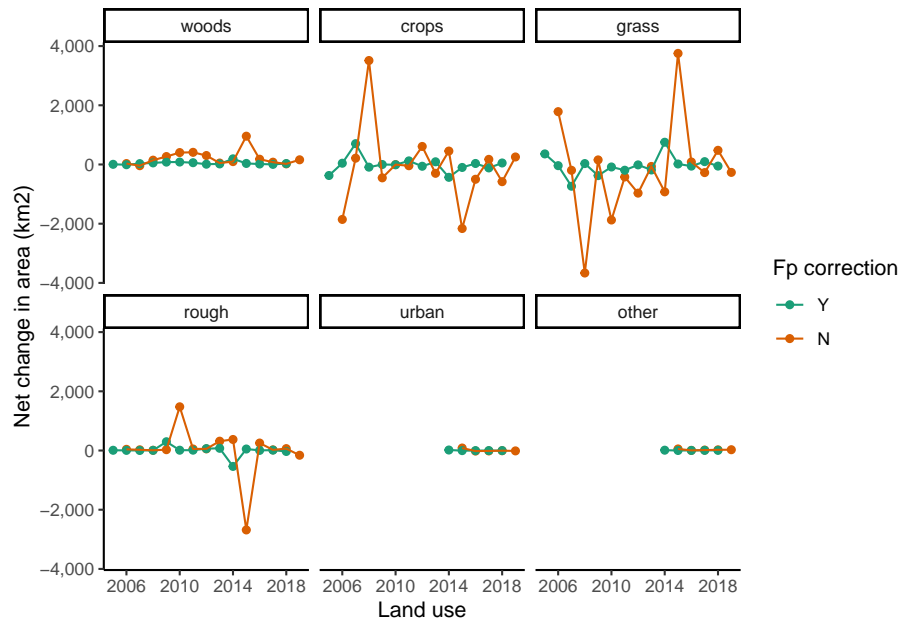
This gave the following outputs which could be incorporated into the data assimilation method:

Data source	Fn	Fp
FC	0.0020230	NA
LCM	0.0013481	0.8711168
CORINE	0.0060332	0.9029868
LCC	0.0012670	0.6737150
IACS	0.0020691	0.7997226
CROME	0.0012571	0.9329713

### 2.5.6 Updating $B, D, G$ and $L$

To incorporate the false positives into the Tracking Land-Use Change data assimilation approach to account for uncertainty in the data-sets, we can apply the false positive rates to the  $B$  transition matrix:  $B * (1-Fp)$ .

The revised  $B$  matrix can then be used to recalculate  $D, G$  and  $L$  for each data source. An example is provided below for IACS from 2005 to 2019:



## 2.6 Conclusions

- Representing data source-specific uncertainty is relatively straightforward in principle. We need to estimate appropriate  $\sigma$  values for each data source and use these in the likelihood function.
- The most fundamental problem is accurately estimating  $\sigma$  in the absence of any data which we regard as “true”, particularly for the  $B$  matrices which are key. There is no immediate solution to this, and a pragmatic approach is to define a reference data set, with more or less subjectivity/expert judgement, and principles from cross-validation.
- A starting point would be to implement a simple method, whereby  $\sigma$  for each data set is scaled according to metrics measuring its correspondence with reference data. This could be based on any or all of  $D, G, L$  and  $B$ .
- A better method is to estimate the biases and uncertainties as part of the data assimilation. With confusion matrices, we have a clear method for doing this, by explicitly representing the false positive and false negative error rates. The downside of this approach is that it is more complicated, involves estimating more parameters, and will have greater computation time.
- Here we have demonstrated the generation of both *sigma* to use as scaling and also the generation of false positive and negative error rates. In both cases, the sticking point remains defining a suitable reference data-set where all of the available data sources, including ground-truthed data, are flawed in some way.
- With this in mind we have calculated data-set level *sigma*,  $F_p$  and  $F_n$  rather than land-use level values.

```
## Computation time (excl. render): 137.34 sec elapsed
```



# Chapter 3

## Assessing systematic errors in estimates of land-use change: sensitivity to survey-interval length

### 3.1 Introduction

The spatial datasets used in the data assimilation for Land Use Tracking will contain systematic errors, related to falsely detecting land-use change when it has not occurred, and missing true land-use change when it does occur. To characterise uncertainties in the data, we want to quantify these false positive and false negative detection rates. These have previously been estimated by comparison with a reference dataset, and thereby judging where the observed changes in a given data set are correctly identified or not. However, this depends on the validity of the reference dataset as a standard for comparison, and we know that the reference data set is imperfect. Here we use an alternative method that assesses these error rates by analysing the apparent rate of land-use change as a function of the time interval between surveys. In the absence of systematic errors, no relationship with survey-interval length would be expected, and any apparent sensitivity can be used to infer the error rates.

The observed area changing from one land-use type  $i$  to another  $j$  between two surveys,  $\beta_{ij}^{\text{obs}}$  (in  $\text{km}^2 \text{ yr}^{-1}$ ), will be made up of the true rate of change,  $\beta_{ij}$  and systematic and random error terms. Systematic errors comprise false positive ( $F^P$ ) and false negative rates ( $F^N$ ). Together with the random error term  $\epsilon_{ij}$ , we can express our expectation for the observations to be:

$$\beta_{ij}^{\text{obs}} = \beta_{ij} + (F_{ij}^P - F_{ij}^N) + \epsilon_{ij} \quad (3.1)$$

As a broad approximation, we can assume that the true rate of land-use change, and the error rates, are approximately constant in time. With short intervals between surveys, there will therefore be proportionately less true change, but the magnitude of the errors will be the same. Conversely, with long intervals between surveys, the magnitude of the errors will still be the same, but there will be proportionately more true change. As the time difference between surveys increases, the observed rate will tend towards an asymptote, equal to the true mean rate of land-use change,  $\bar{\beta}_{ij}$ , as the random error term  $\epsilon_{ij}$  has a mean of zero. We can therefore examine the apparent rate of land-use change as a function of the time interval between surveys, and infer the error rates from this relationship. It is not possible to explicitly separate  $F^P$  and  $F^N$  in this analysis, only their net effect  $F^{\text{net}} = F^P - F^N$ , although the shape of curve indicates which is larger in the data. If  $F^P$  and  $F^N$  were zero, or exactly balancing each other, the data would show a flat line in the figures below. For the datasets we are testing here, in all cases it appears that false positives are the major source of error.

This method is potentially superior to estimating error rates by comparison with a reference dataset, as it does not require reliable ground-truth data, and only uses intrinsic properties of the observations. As a down-side, the error rates calculated apply to ongoing directional change, and any rotational change is effectively included in the error term. However, we note that this is only really an issue with crop-grass transitions (and v.v.), and we estimate, this affects around  $\sim 7\%$  of the grassland area (assuming that half the area of grassland  $< 5$  years old has a rotation length shorter than the observation period). The method also assumes that the true mean rate of land use change has not changed systematically over the observation period.

## 3.2 Methods

- Calculate beta matrices for land-use change with all possible permutations of between-survey intervals available with each data source
- Plot the relationship between time-interval length ( $\Delta$ ) and the apparent rate of land-use change
- For each term in the  $\beta$  matrix, we fit an exponential model to the data using nonlinear least squares:

$$\beta_{ij\Delta}^{\text{obs}} = \bar{\beta}_{ij} + (A_0 - \bar{\beta}_{ij})\exp(-\exp(k)\Delta) \quad (3.2)$$

where  $\bar{\beta}_{ij}$  is the asymptotic value, equal to the long-term mean rate of land-use change,  $A_0$  is the intercept at  $\Delta = 0$ , and  $k$  is the natural logarithm of the rate constant.

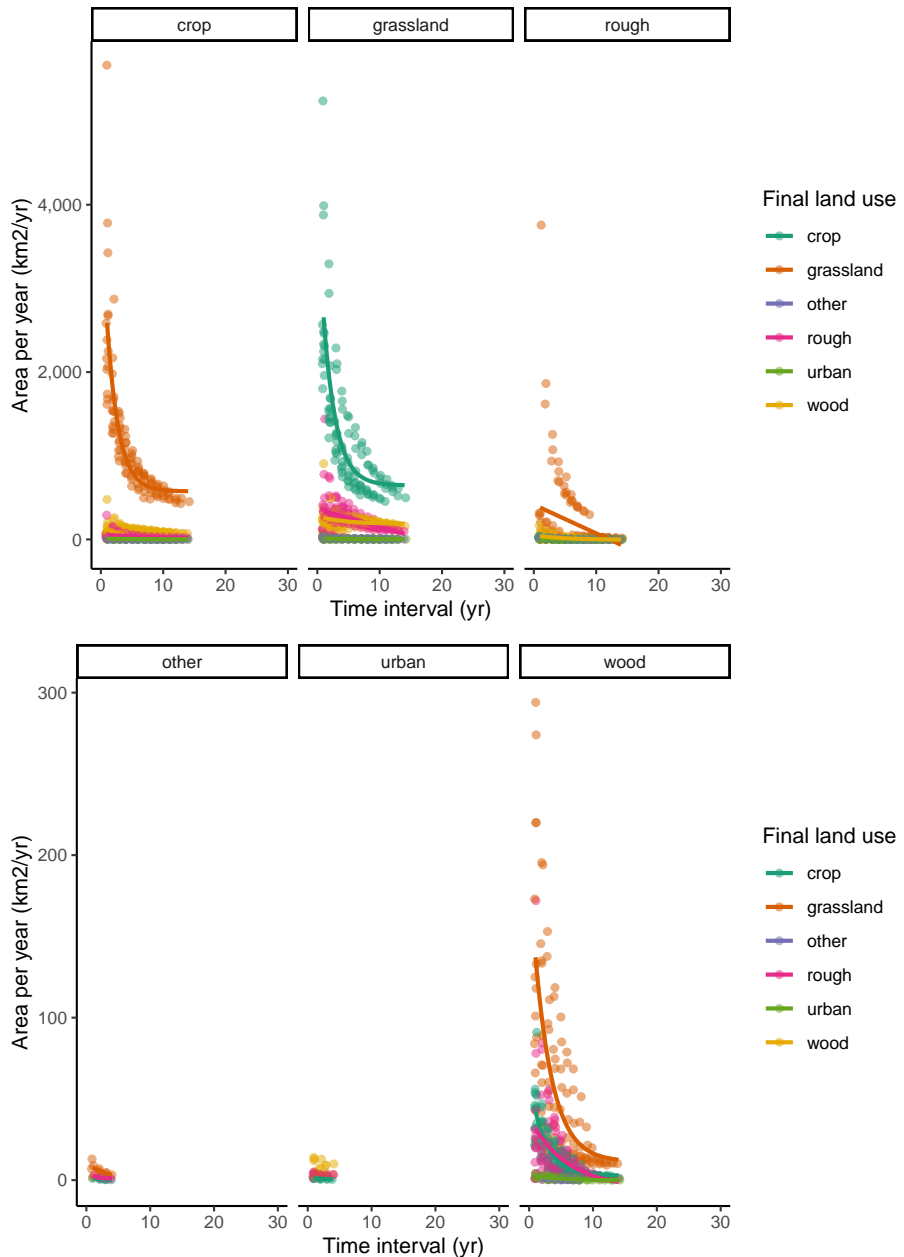
From the fitted model, we obtain estimates of  $\overline{\beta_{ij}}$  and the value of  $\beta_{ij\Delta}^{obs}$  as a function of the time interval  $\Delta$ . We can then estimate the mean net error rate for a given time interval from the fitted curve, expressing this as a fraction of the observed rate:

$$F_{ij\Delta}^{\text{net}} = (\beta_{ij\Delta}^{\text{obs}} - \overline{\beta_{ij}}) / \beta_{ij\Delta}^{\text{obs}} \quad (3.3)$$

### 3.3 Results

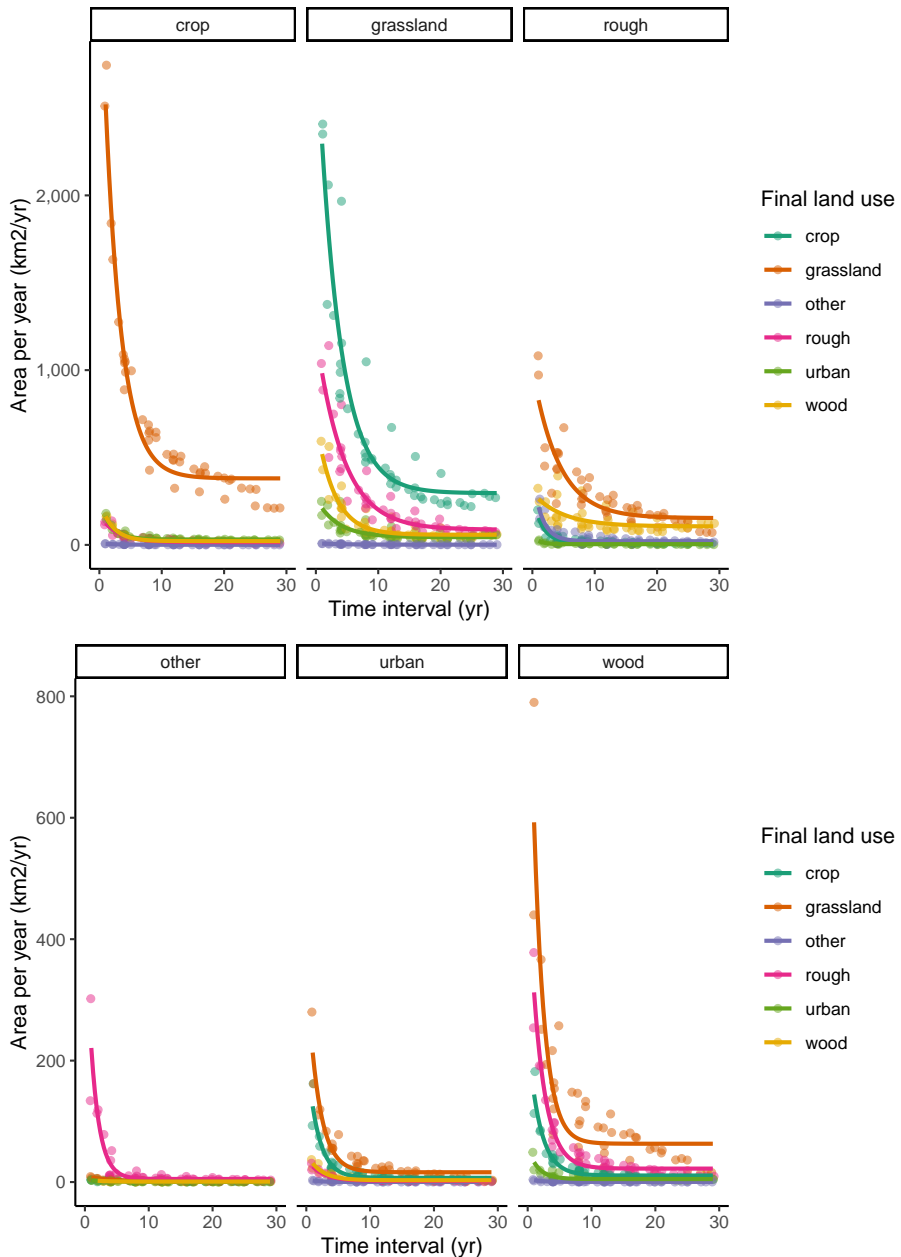
In almost all cases, we see very strong sensitivity to survey-interval length, with much higher apparent rates of change observed at short interval lengths. This implies the observations are dominated by false positives; no relationship would be expected in the absence of such errors. Similar trends are seen in all the data sets examined here.

### 3.3.1 IACS:



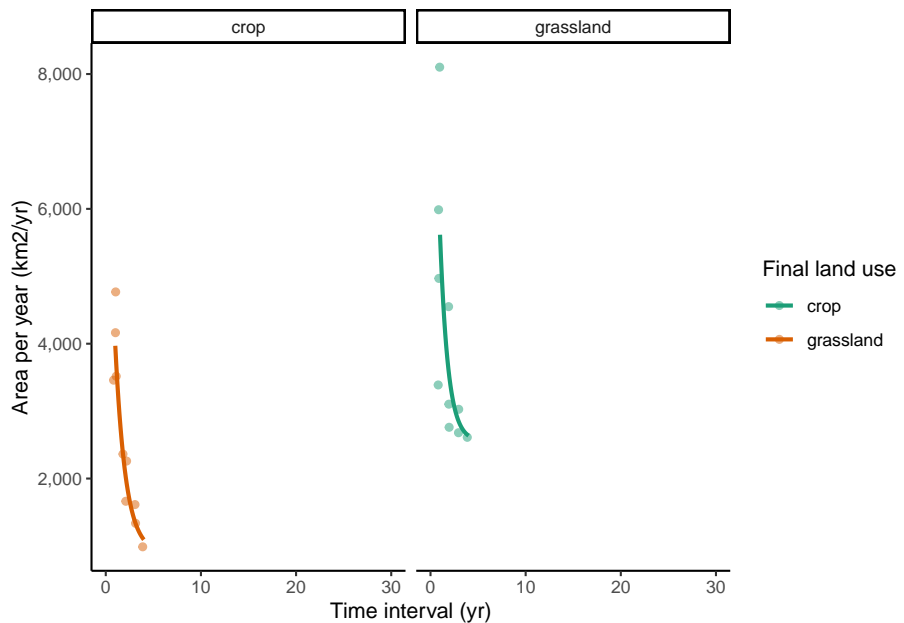
### 3.3.2 LCM

LCM has the greatest number of datasets to apply this method to with 10 surveys conducted across 29 years. This enables comparison between surveys that give 23 time intervals.



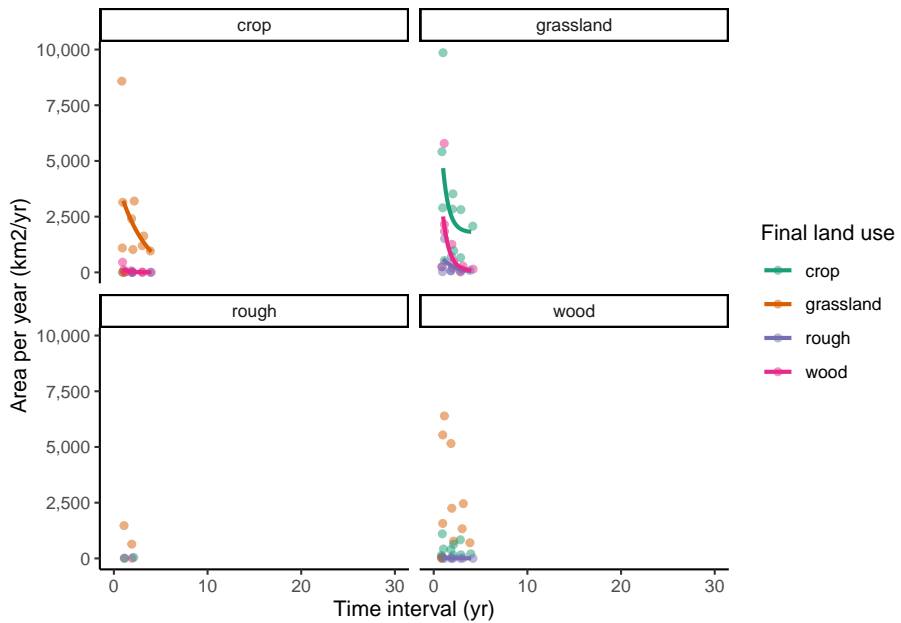
### 3.3.3 LCC:

LCC only includes crop and grassland land use change so there are less data to test.

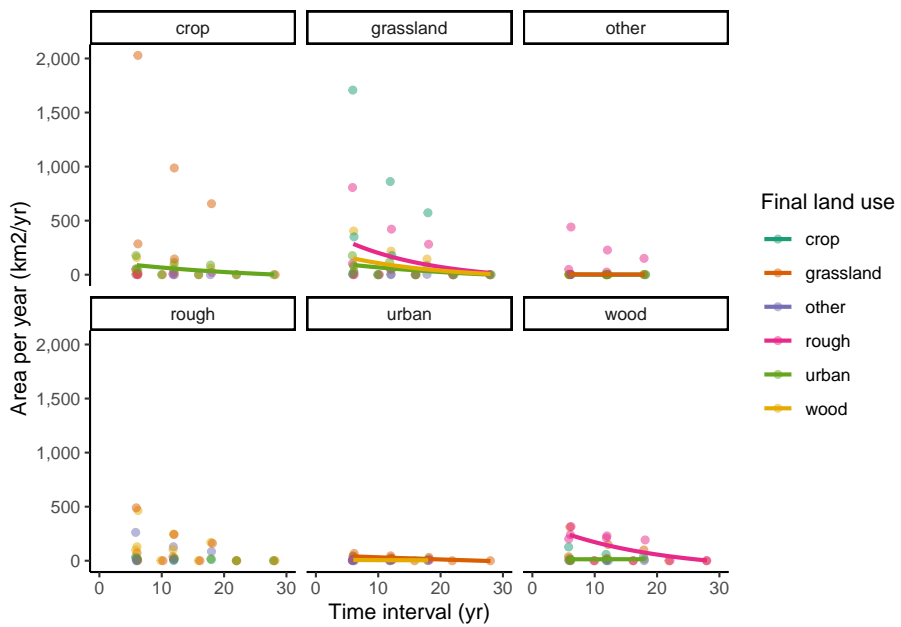


### 3.3.4 CROME:

Both CROME and CORINE have few surveys meaning estimating a fit to this data is difficult:



### 3.3.5 CORINE:

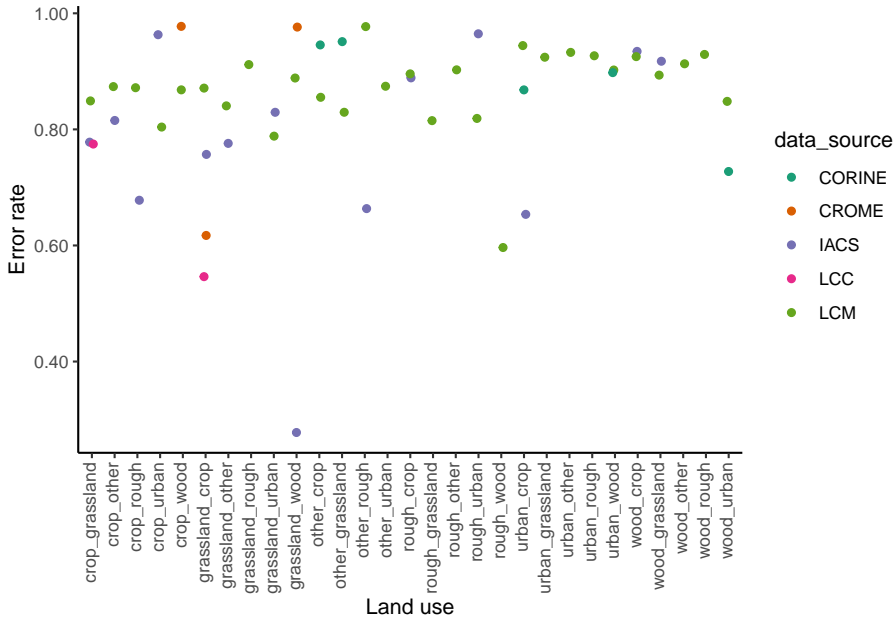


### 3.3.6 Summary Table

The table below shows the error rate for all of the different land use change categories for each of the different data sets. These are calculated for the typical time interval in each of the different data sources.

luc	IACS	LCM	LCC	CORINE	CROME
crop_grassland	0.78	0.85	0.77	NA	NA
crop_other	0.82	0.87	NA	NA	NA
crop_rough	0.68	0.87	NA	NA	NA
crop_urban	0.96	0.80	NA	NA	NA
grassland_crop	0.76	0.87	0.55	NA	0.62
grassland_other	0.78	0.84	NA	NA	NA
grassland_urban	0.83	0.79	NA	NA	NA
grassland_wood	0.28	0.89	NA	NA	0.98
other_rough	0.66	0.98	NA	NA	NA
rough_crop	0.89	0.90	NA	NA	NA
rough_urban	0.96	0.82	NA	NA	NA
urban_crop	0.65	0.94	NA	0.87	NA
wood_crop	0.93	0.93	NA	NA	NA
wood_grassland	0.92	0.89	NA	NA	NA
crop_wood	NA	0.87	NA	NA	0.98
grassland_rough	NA	0.91	NA	NA	NA
other_crop	NA	0.86	NA	0.95	NA
other_grassland	NA	0.83	NA	0.95	NA
other_urban	NA	0.87	NA	NA	NA
rough_grassland	NA	0.82	NA	NA	NA
rough_other	NA	0.90	NA	NA	NA
rough_wood	NA	0.60	NA	NA	NA
urban_grassland	NA	0.92	NA	NA	NA
urban_other	NA	0.93	NA	NA	NA
urban_rough	NA	0.93	NA	NA	NA
urban_wood	NA	0.90	NA	0.90	NA
wood_other	NA	0.91	NA	NA	NA
wood_rough	NA	0.93	NA	NA	NA
wood_urban	NA	0.85	NA	0.73	NA

The figure below shows the same data plotted for all data sources.



### 3.4 Discussion and Conclusions

The error rates we obtain from this method are similar to those derived from comparison with the reference data set. The net positive error rates are generally in the range 80-98 %; that is, 80-98 % of the ostensibly observed land-use change did not actually occur. Almost all other values in the range 50-80 % (with only one exception less than this). The conclusion from this is that these observations are extremely over-sensitive, and for whatever reason, differences in imagery (or survey data in the case of IACS) at different times is being recorded as land-use change when none has occurred.

This makes it challenging to extract useful information from these data. However, if we believe the error rates to be consistent, we can specify and correct for these errors in the data assimilation procedure, as described previously. Land-use-change-specific rates can be estimated from this analysis, to capture the variability in errors between different land-use conversions. However, the error rates are broadly similar, and a single value per data source could justifiably be used. To explore this further, confidence intervals can also be calculated for the error rates in the table above, using the standard errors in the parameters from the exponential model fit. If the errors are not consistent in time, and given their magnitude of 80-98 %, an alternative conclusion would be that these observations are not yet reliable enough to include in the inventory procedure for tracking land-use change.



# Chapter 4

## Estimating false-positive rates in detection of land-use change based on classification accuracy

### 4.1 Introduction

In the “Tracking Land-Use Change” project, several data sources provide a time series of maps of land use. An obvious approach is to estimate land-use change as the difference between these maps over time. However, any error in land classification will also be included in the estimate of land-use change, so it is important to quantify these errors properly and note how they propagate. Here, we show the calculations which propagate the error in classification through to its resulting effect on the estimate of land-use change.

### 4.2 Methods

The accuracy of land-use maps is usually estimated by comparison with some reference data set. We can then calculate confusion matrices and metrics of overall agreement, of which there are several. Common choices are overall accuracy ( $\alpha$ , the fraction of locations where estimated land use agrees with the reference data set) and the  $\kappa$  statistic, which corrects for the probability of chance agreement.  $\kappa$  therefore gives a more robust measure, typically 5-20 % lower than simple percentage agreement. The probability of misclassification can be estimated simply as  $1 - \alpha$  or more stringently as  $1 - \kappa$ . For maps at times  $t_1$  and  $t_2$ , the probabilities of misclassification are denoted  $p_1$  and  $p_2$ . Estimating

land-use change involves calculating the difference between maps, and the errors are additive in the result. The probability of estimating erroneous land-use change because of misclassification in a pair of maps can be written as

$$p_{1\cup 2} = p_1 + p_2 - p_{1\cap 2}. \quad (4.1)$$

That is, the probability of error is the union of two events (misclassification occurring at time 1 or at time 2, minus their intersection  $p_{1\cap 2}$ , which is the probability of misclassification at both time 1 and time 2, which would otherwise be double-counted.  $p_{1\cap 2}$  can be estimated as  $p_1 p_2$  assuming that the errors leading to misclassification at times 1 and 2 are independent of each other. In practice, our estimates of the probabilities of misclassification at times 1 and 2 are usually the same ( $p_1 \approx p_2$ ), so this simplifies to:

$$p_{1\cup 2} = 2p_1 - p_1^2. \quad (4.2)$$

### 4.3 Results

Estimates of  $\alpha$  and  $\kappa$  from some of the data sets used in the LUC Tracking project are shown in the table below.

Data source	$\alpha$	$\kappa$
Corine	0.80	0.64
LCC	0.91	0.82
LCM	0.88	NA

For the purposes of the examples below, we use the value of 0.88, the overall accuracy of the LCM, as a relatively optimistic metric. The value of  $p_1 \approx p_2$  is  $1 - \alpha$ , and therefore  $= 0.12$ .

Using this value in Equation 4.2 yields a probability of estimating erroneous land-use change because of misclassification of 0.226. Because this probability applies at every location on the map, multiplying by the total area yields the expected area of erroneous land-use change. So, when comparing two UK maps which each have a classification accuracy of 88 %, 22.6 % of the area, around 55000 km<sup>2</sup>, will show land-use change where none actually occurs. This provides a huge amount of measurement noise when we are attempting to detect a very small signal: the expected magnitude of actual land use change in the UK is of the order of a few hundred km<sup>2</sup>, and at most a few thousand km<sup>2</sup>, based on Forestry Commission planting rates, Agricultural Census, and urban expansion data. The area of land changing use is thus less than 1 % of the total area, and we would therefore need the probability of misclassification error to be less than this in order to accurately detect true change (meaning the accuracy needs to be > 99 %).

We can extend this to calculate the false positive rates for terms in the  $\beta$  matrix and gross gains and losses, given the appropriate denominators and estimates of the true extent of land-use change. For example, the area of cropland in England is approximately 45000 km<sup>2</sup>, and the area of gross gains and losses are estimated to be in the range 300-800 km<sup>2</sup> y<sup>-1</sup> based on CS. Based on the June Agricultural Census, we might estimate these rates to be higher, perhaps reaching 1000-3000 km<sup>2</sup> y<sup>-1</sup>.

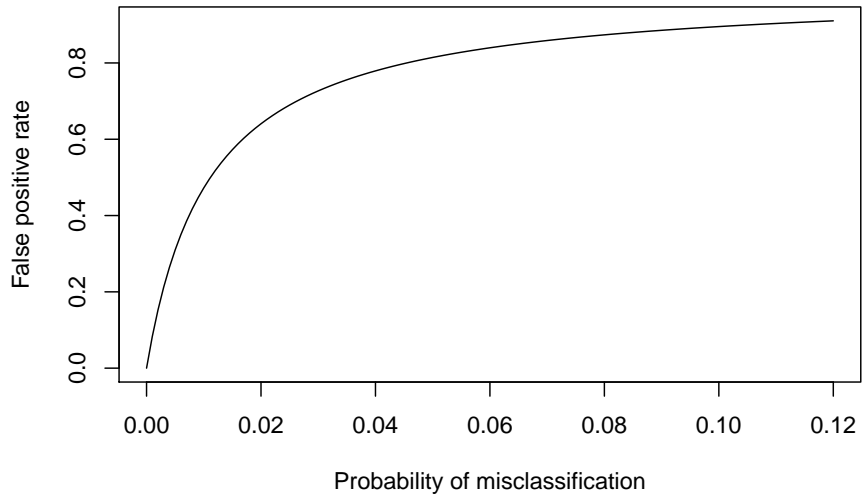
Expressing the estimated true land-use change  $A_{true}$  as a fraction of the total recorded land-use change (i.e. true + erroneous), we can calculate the relevant false positive rate,  $F_P$ .

$$F_P = 1 - \frac{A_{true}}{A_{true} + A_{false}} \quad (4.3)$$

If CS rates of land-use change are correct (300-800 km<sup>2</sup> y<sup>-1</sup>), the false positive rate is in the range 92.7 to 97.1 %.

If the Agricultural Census rates of land-use change are correct (1000-3000 km<sup>2</sup> y<sup>-1</sup>), the false positive rate is in the range 77.2 to 91 %.

Given this relationship between the classification accuracy of individual maps and the resulting false positive rates in detecting land-use change, we can examine the improvement needed to obtain false positive rates below a given level. The figure below shows the change in false positive rate with classification error (1- $\alpha$ ), using the example of cropland gains in England as above, assuming a true rate of change of 1000 km<sup>2</sup> y<sup>-1</sup>.



The figure shows asymptotic behaviour because of the form of Equation 4.3, with a constant true area expressed with an increasing  $A_{false}$  term in the denominator. The result is that it takes a substantial decrease in misclassification (or increase in accuracy) from present values to achieve a marked increase in the false positive rate. For example, to reduce the false positive rate to 0.5 requires an accuracy of 0.988. The basic problem is that the true areas of change are very small compared to current error rates, and it would require an order of magnitude improvement in accuracy to reduce the measurement noise to a similar level to the signal we want to detect.

## 4.4 Conclusions

- Accuracy of land-use classification is in the range 0.8-0.9 in the available data sets. The corresponding probability of misclassification is 10-20 %.
- The errors in individual maps can be propagated to calculate the error in their differences i.e. estimates of land-use change.
- Error rates for land-use change propagating from misclassification will typically be greater than 20 %. This is 1-2 orders of magnitude larger than the expected land-use change.
- The probability of misclassification can be used to calculate the false positive rate of land-use change detection, and values are typically around 90 %.
- Whilst these errors are predictable and can be accounted for, directly detecting the expected land-use change rates <1 % is not currently practi-

cable.



# Chapter 5

## Using life tables in modelling land-use change

### 5.1 Introduction

This section describes the concept of life tables in modelling land-use change. In the current procedure, we firstly estimate the  $B$  matrix each year by MCMC, then estimate where these land-use changes take place in a separate step. This second step uses static maps of likelihood for each land use. That is, for each year, we have a raster containing the likelihood of a given land-use occurring in each cell. This is based on observed data; if several data sets agree that a given cell is used for crops in a given year, there is a high likelihood of any new cropland being placed there by the algorithm (if it is not already cropland). However, these likelihood maps are static: they vary over time according to the data, but they are the same in every simulation. What this misses is the dependence of land-use change on prior history in the grid cell. There are a few cases where this is important. Most importantly, there is rotational grassland, which is used for arable crops for a number of years, before being returned to grassland on a repeating cycle. Thus, the likelihood of grassland changing to cropland is higher for a four-year old grassland than a 50-year old grassland. This phenomenon is not well captured in the current method. For forests, deforestation may be more likely to occur where the trees are at a commercially harvestable age, so the likelihood of transition is not constant, but peaks at around 40-60 years. More generally, land use shows inertia, and change is less likely where no change has happened before.

To capture such “memory” effects (i.e. that the time since past land-use change affects the likelihood of current land-use change), we can use an approach borrowed from population modelling based on “life tables”. In the population modelling context, life tables are a set of age-specific mortality rates. The

same idea is referred to as survival analysis, reliability analysis, or time-to-event analysis in various domains. Here, we are modelling the “survival” of land under a given continuous usage. Using the population analogy, a forest is “born” when a grid cell is afforested (from any other previous land use), and “dies” when it is deforested (converted to any other previous land use). Similarly, the same applies when areas of other land uses are created or destroyed. We can think of this as six populations (woods, cropland, grassland, rough grazing, urban or other land uses), each of which has a specific life table. In this context, rather than mortality rates, the life table is the set of age-specific probabilities of conversion to other uses. So rather than a single dimension, each life table has six columns, for the probabilities to conversion to each of the five other land uses, plus the probability of remaining unchanged.

## 5.2 Illustration with dummy data

To illustrate the idea, we can make up some dummy data which shows how this might work.

The life table for grassland over the first ten years might look like the below. The mortality/transition probabilities are usually denoted  $\lambda$ .

```
knitr:::kable(data.frame(time = 1:10, a_lamda[1:10, u_from, 1:n_u]))
```

time	woods	crops	grass	rough	urban	other
1	0.01	0.03	0.93	0.02	0.01	0
2	0.01	0.05	0.91	0.02	0.01	0
3	0.01	0.10	0.86	0.02	0.01	0
4	0.01	0.12	0.84	0.02	0.01	0
5	0.01	0.06	0.90	0.02	0.01	0
6	0.01	0.03	0.93	0.02	0.01	0
7	0.01	0.03	0.93	0.02	0.01	0
8	0.01	0.03	0.93	0.02	0.01	0
9	0.01	0.03	0.93	0.02	0.01	0
10	0.01	0.03	0.93	0.02	0.01	0

This shows that grassland will typically remain grassland, but that it has a higher chance of being converted to cropland in years 2-5. The chance of other conversions remains constant. For efficient computation, we can store the  $\lambda$  values in a three-dimensional array, which allows us to access the values, referencing by index.

```
# e.g. if we want to know the prob of 4-y old grass turning to crop
t = 4; u_from = 3; u_to = 2
a_lamda[t, u_from, u_to]
```

```
## [1] 0.12
```

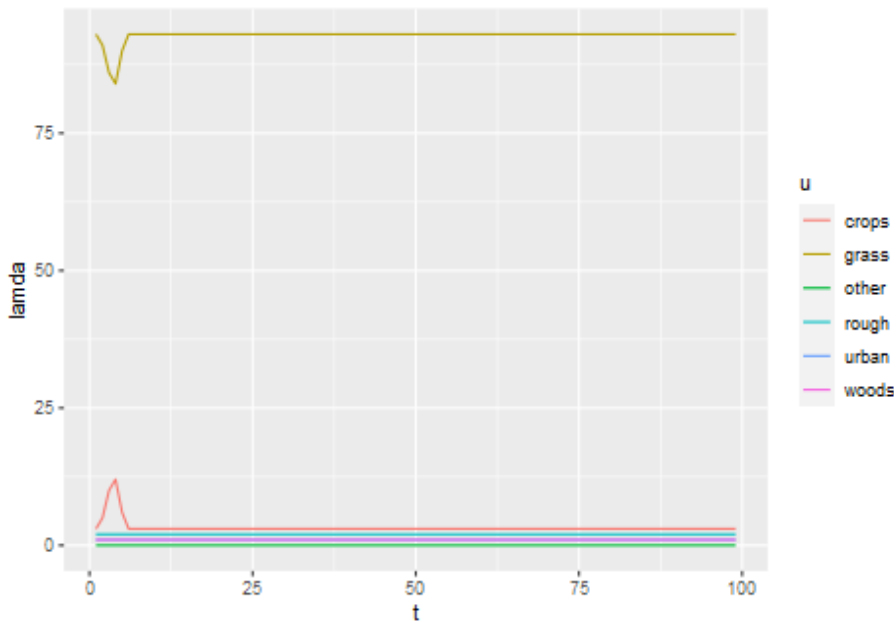
We can plot the grassland dummy data as an example.

```

df <- df3
df$u <- NULL
df$t <- as.numeric(rownames(df))
df <- pivot_longer(df,
  cols = woods:other,
  names_to = "u",
  values_to = "lamda")

p <- ggplot(df, aes(t, lamda, colour = u))
p <- p + geom_line()
#p <- p + facet_wrap(~ u, scale = "fixed")
p

```



### 5.3 Next steps

To use this idea in the LUC Tracking project, there are several steps required.

1. Establish the life tables, based on observed data. This requires writing functions to extract and analyse all the “life spans” in a set of vectors or  $U$  stack object. This means counting frequency distribution of all the length of all contiguous land uses.
2. Establishing the age-of-land-use for the starting point map (2019).
3. Adapting the code in DA4\_SampleU.Rmd to use the life tables dynamically

to calculate the likelihoods  $\mathcal{L}$  in sampling  $U$ , going back in time from 2019. Previously, this was done in a single step in DA3\_LikelihoodU.Rmd, to calculate a number of static maps. This would now need to be done dynamically, multiplying the spatial likelihood term  $\mathcal{L}_{\text{static}}$  with the dynamic likelihood term  $\mathcal{L}_{\text{dynamic}}$  (depending on the age of the current land use). Because  $\mathcal{L}_{\text{dynamic}}$  depends only on the age (and not the whole previous history), we simply need to update a raster containing the age of each land use each year. This will start with the estimate from step 2 and work backwards.

```
## Computation time (excl. render): 1.53 sec elapsed
```

## Chapter 6

# Results: England

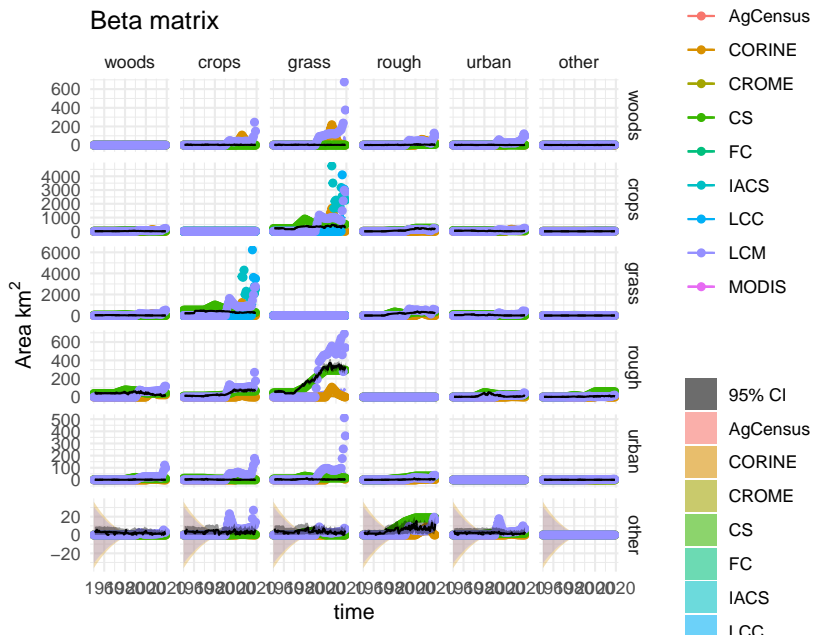


Figure 6.1: Observations and posterior distribution of the transition matrix  $\mathbf{B}$ , representing the gross area changing from the land use in each row to the land use in each column each year from 1950 to 2020. The grey shaded band shows the 2.5 and 97.5 percentiles of the posterior distribution. The maximum *a posteriori* estimate is shown as the solid black line within this. Observations from the different data sources are shown as coloured circles. The coloured solid lines show the corrected observations after accounting for systematic uncertainties, and interpolating. The coloured bands around these lines show the random uncertainty, rescaled as  $\sigma/5$  to keep with the axis scale. Because the random uncertainties and the corrections to the observations are generally very large in comparison to the actual change, scaling the axes is difficult. Note that a consistent colour scheme for the data sources is shown, but not all contribute to every figure.

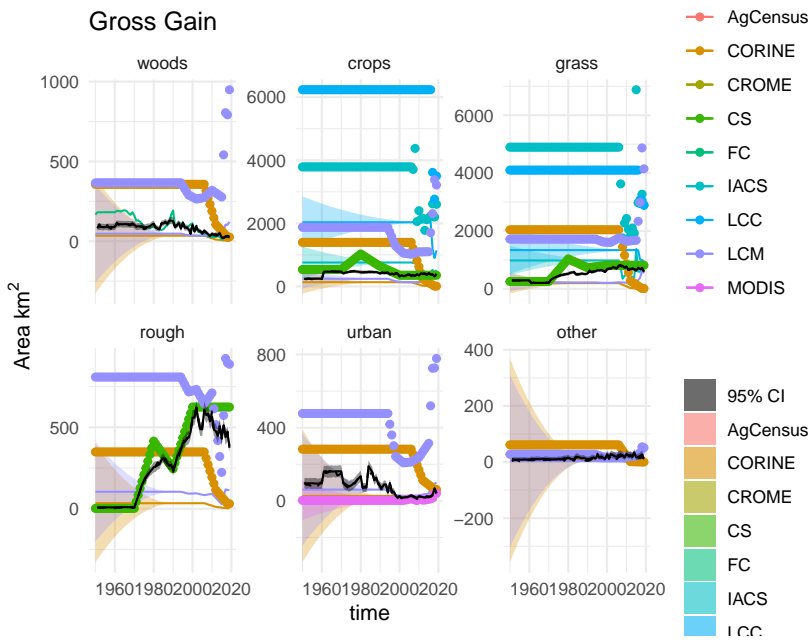


Figure 6.2: Observations and posterior distribution of the gross gain in area of each land use  $\mathbf{G}$  from 1950 to 2020. The grey shaded band shows the 2.5 and 97.5 percentiles of the posterior distribution. The maximum *a posteriori* estimate is shown as the solid black line within this. Observations from the different data sources are shown as coloured circles. The coloured solid lines show the corrected observations after accounting for systematic uncertainties, and interpolating. The coloured bands around these lines show the random uncertainty, rescaled as  $\sigma/5$  to keep with the axis scale. Because the random uncertainties and the corrections to the observations are generally very large in comparison to the actual change, scaling the axes is difficult. Note that a consistent colour scheme for the data sources is shown, but not all contribute to every figure.

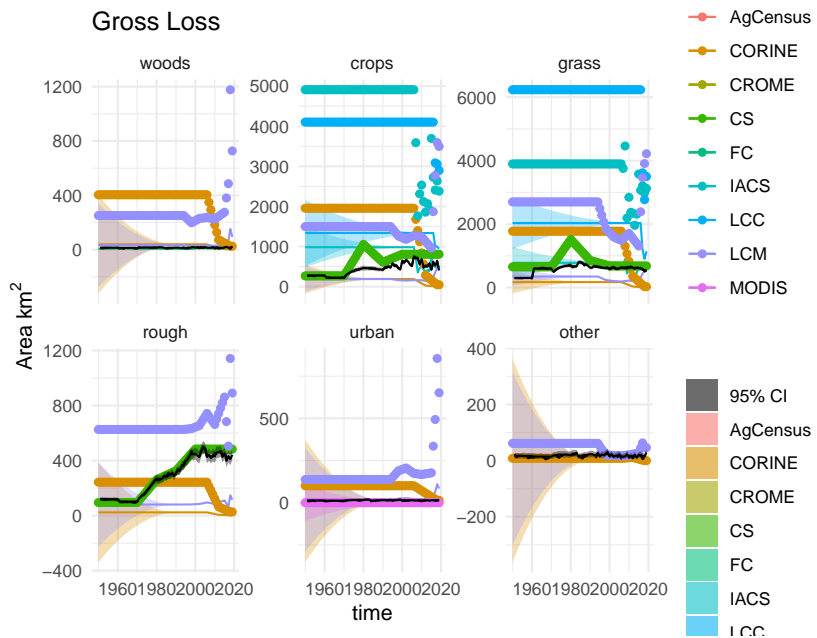


Figure 6.3: Observations and posterior distribution of the gross loss of area from each land use  $\mathbf{L}$  from 1950 to 2020. The grey shaded band shows the 2.5 and 97.5 percentiles of the posterior distribution. The maximum *a posteriori* estimate is shown as the solid black line within this. Observations from the different data sources are shown as coloured circles. The coloured solid lines show the corrected observations after accounting for systematic uncertainties, and interpolating. The coloured bands around these lines show the random uncertainty, rescaled as  $\sigma/5$  to keep with the axis scale. Because the random uncertainties and the corrections to the observations are generally very large in comparison to the actual change, scaling the axes is difficult. Note that a consistent colour scheme for the data sources is shown, but not all contribute to every figure.

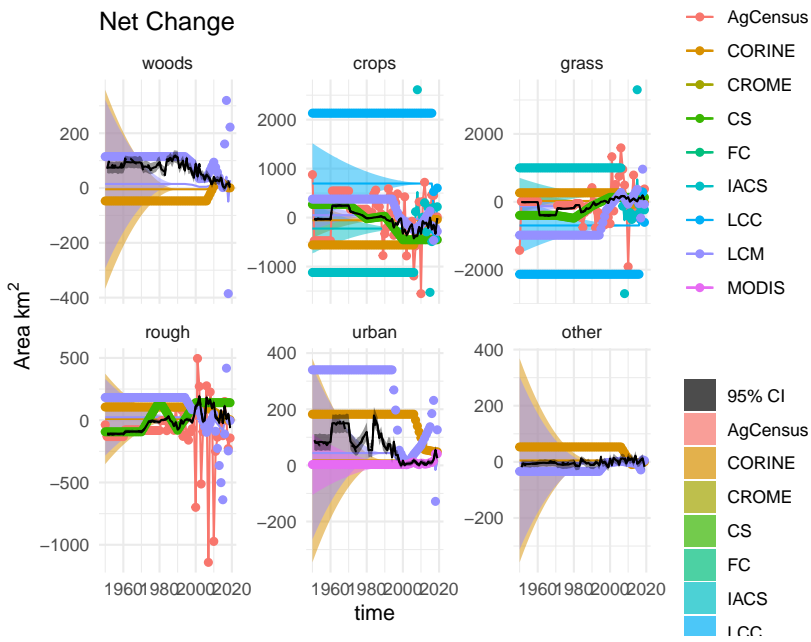


Figure 6.4: Time series of the net change in area occupied by each land use ( $D$ ) from 1950 to 2020, showing the observations and posterior distribution of estimates. The grey shaded band shows the 2.5 and 97.5 percentiles of the posterior distribution. The maximum *a posteriori* estimate is shown as the solid black line within this. Observations from the different data sources are shown as coloured circles. The coloured solid lines show the corrected observations after accounting for systematic uncertainties, and interpolating. The coloured bands around these lines show the random uncertainty, rescaled as  $\sigma/5$  to keep with the axis scale. Because the random uncertainties and the corrections to the observations are generally very large in comparison to the actual change, scaling the axes is difficult. Note that a consistent colour scheme for the data sources is shown, but not all contribute to every figure.

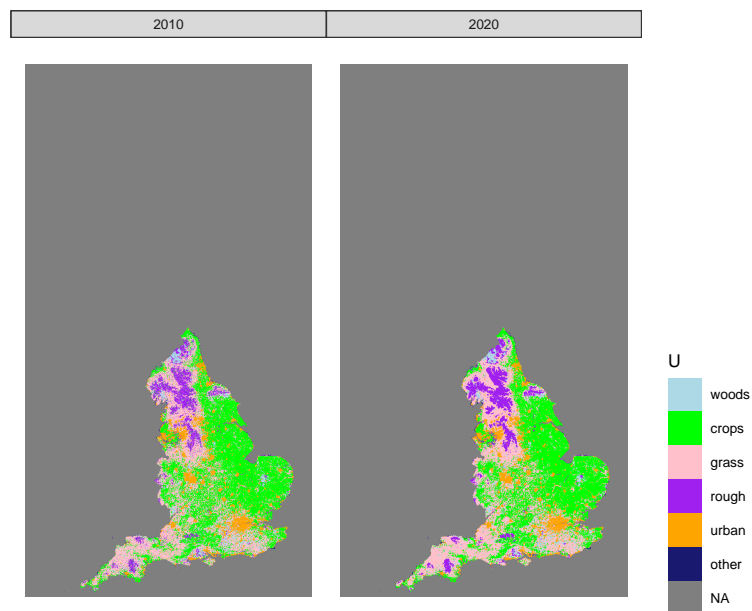


Figure 6.5: Estimated state of land-use in 2010 and 2020 in one realisation of  $U$  from the maximum *a posteriori* estimate of  $B$ .

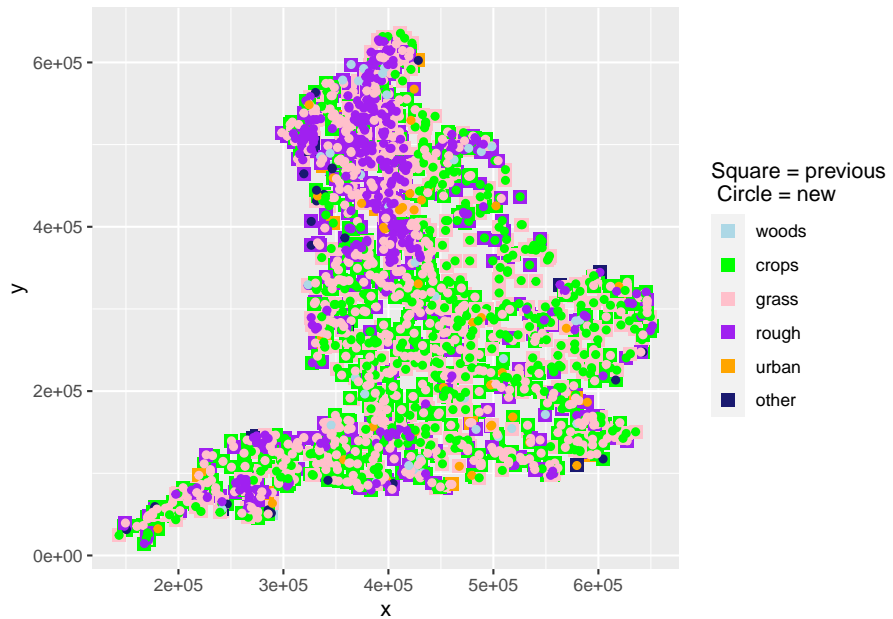


Figure 6.6: The spatial distribution of land-use change between 2010 and 2020 in one realisation of  $U$  from the maximum *a posteriori* estimate of  $B$ . At each location where land use has changed, the use in 2010 is shown as a coloured square, and the use in 2020 is shown as a coloured circle within this

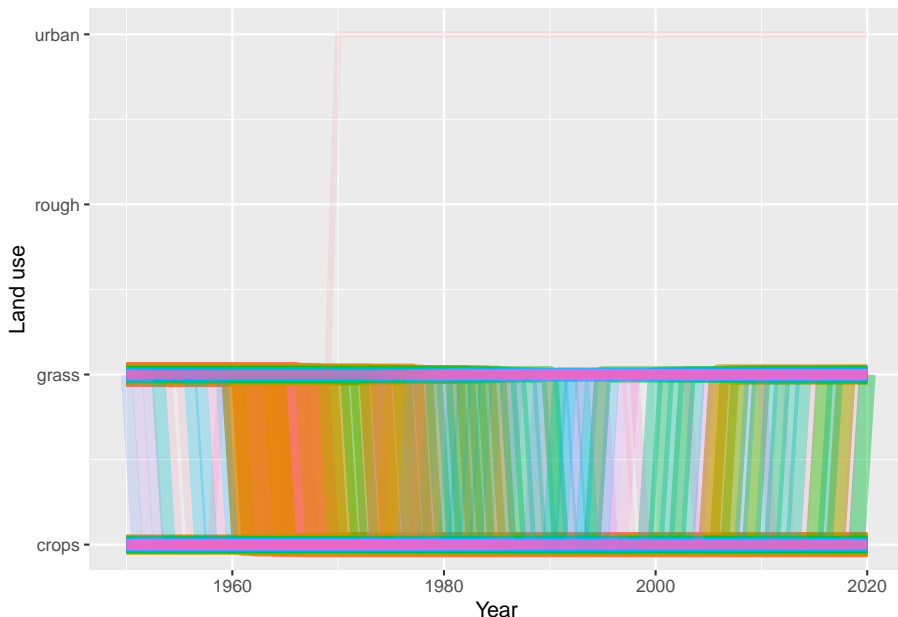


Figure 6.7: Trajectories of the 100 land-use vectors in the posterior  $U$  with the largest areas (excluding the six vectors which show no change). Each vector of land use is shown in a different colour, varied arbitrarily to differentiate different vectors. Line thickness and opacity are proportional to the total area occupied by each vector, so that the dominant vectors are the most visually obvious.

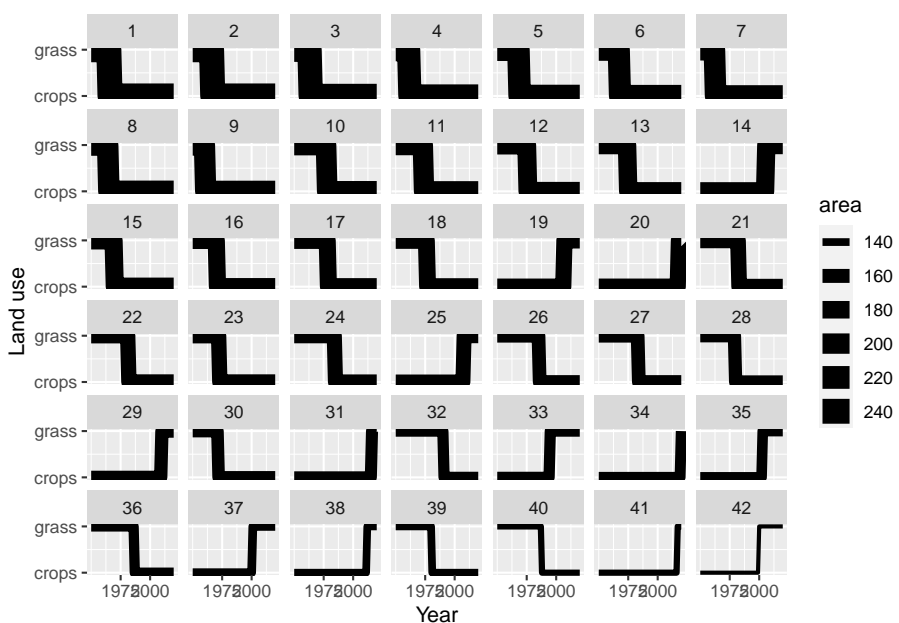


Figure 6.8: Trajectories of the 42 land-use vectors in the posterior  $U$  with the largest areas (excluding the six vectors which show no change). Line thickness is proportional to the total area occupied by each vector.

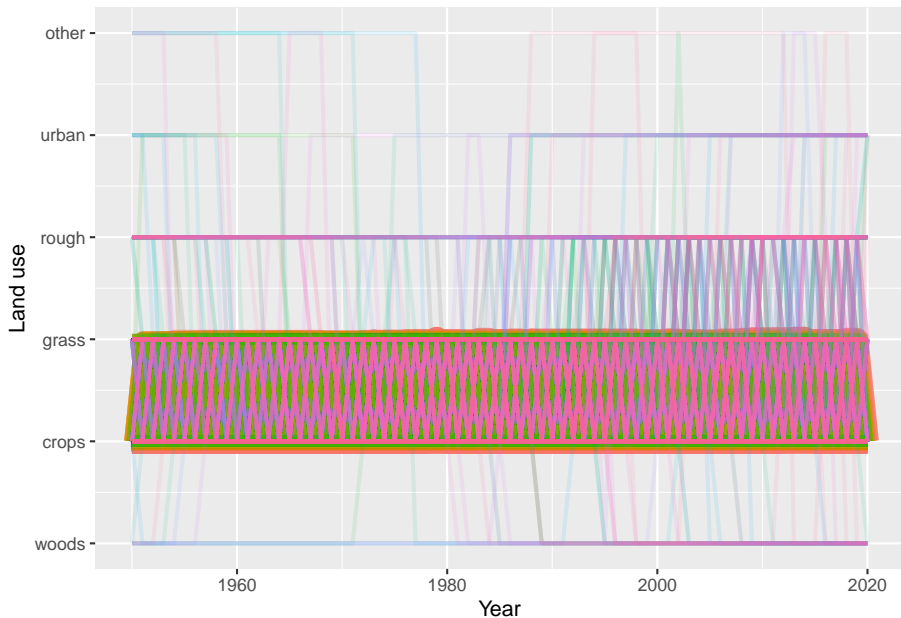


Figure 6.9: Trajectories of the land-use vectors in the posterior  $U$  which involve rotational change between crop and grassland (i.e. those which include either (i) transitions from crop to grass and then subsequently from grass to crop, or (ii) transitions from grass to crop and then subsequently from crop to grass). Each vector of land use is shown in a different colour, varied arbitrarily to differentiate different vectors. Line thickness and opacity are proportional to the total area occupied by each vector, so that the dominant vectors are the most visually obvious.

## Chapter 7

# Results: Scotland

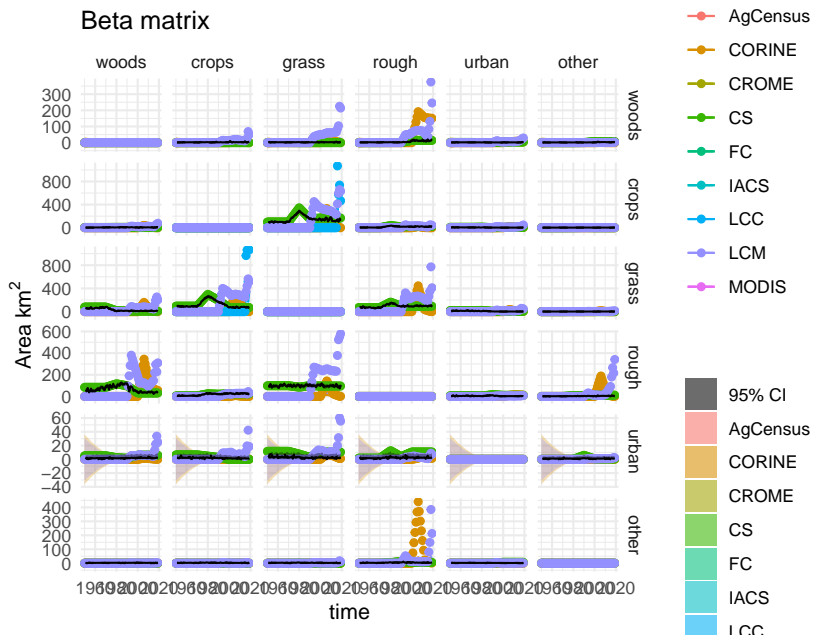


Figure 7.1: Observations and posterior distribution of the transition matrix  $\mathbf{B}$ , representing the gross area changing from the land use in each row to the land use in each column each year from 1950 to 2020. The grey shaded band shows the 2.5 and 97.5 percentiles of the posterior distribution. The maximum *a posteriori* estimate is shown as the solid black line within this. Observations from the different data sources are shown as coloured circles. The coloured solid lines show the corrected observations after accounting for systematic uncertainties, and interpolating. The coloured bands around these lines show the random uncertainty, rescaled as  $\sigma/5$  to keep with the axis scale. Because the random uncertainties and the corrections to the observations are generally very large in comparison to the actual change, scaling the axes is difficult. Note that a consistent colour scheme for the data sources is shown, but not all contribute to every figure.

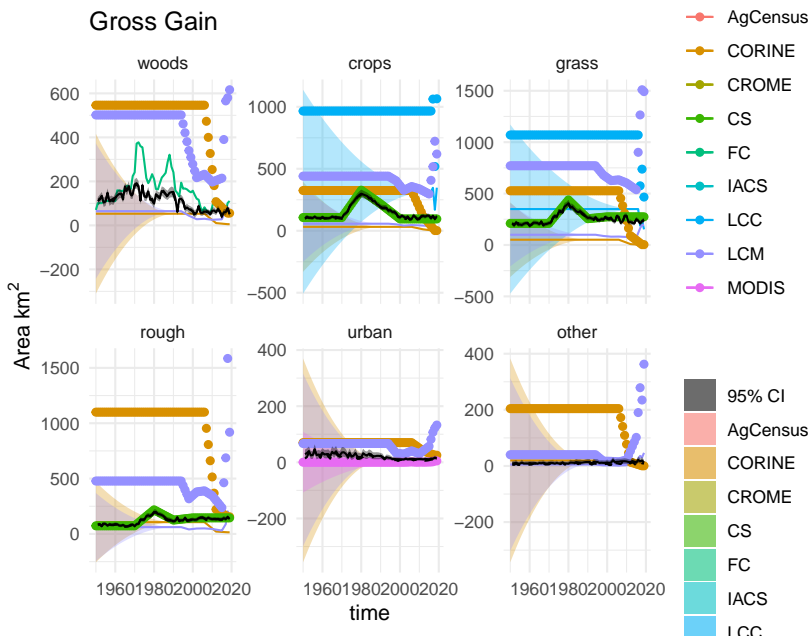


Figure 7.2: Observations and posterior distribution of the gross gain in area of each land use  $\mathbf{G}$  from 1950 to 2020. The grey shaded band shows the 2.5 and 97.5 percentiles of the posterior distribution. The maximum *a posteriori* estimate is shown as the solid black line within this. Observations from the different data sources are shown as coloured circles. The coloured solid lines show the corrected observations after accounting for systematic uncertainties, and interpolating. The coloured bands around these lines show the random uncertainty, rescaled as  $\sigma/5$  to keep with the axis scale. Because the random uncertainties and the corrections to the observations are generally very large in comparison to the actual change, scaling the axes is difficult. Note that a consistent colour scheme for the data sources is shown, but not all contribute to every figure.

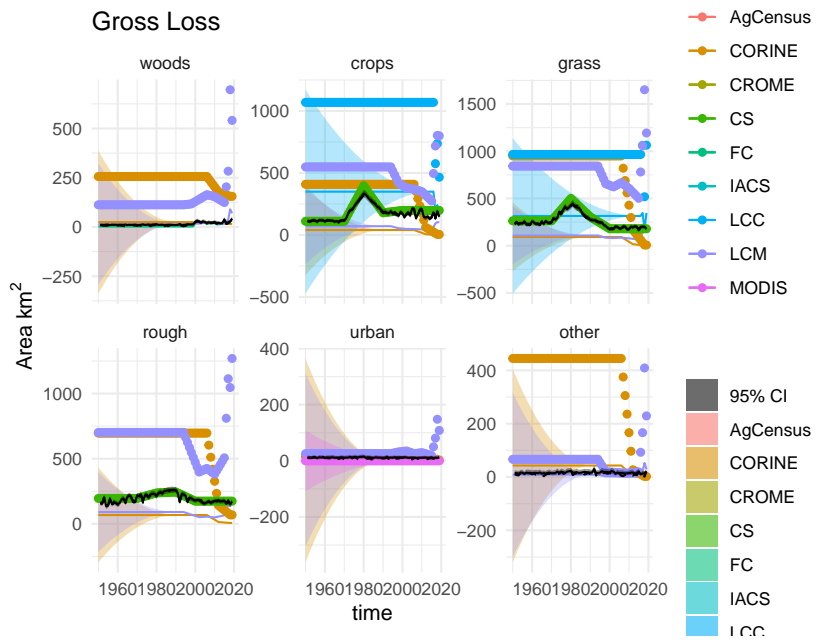


Figure 7.3: Observations and posterior distribution of the gross loss of area from each land use  $\mathbf{L}$  from 1950 to 2020. The grey shaded band shows the 2.5 and 97.5 percentiles of the posterior distribution. The maximum *a posteriori* estimate is shown as the solid black line within this. Observations from the different data sources are shown as coloured circles. The coloured solid lines show the corrected observations after accounting for systematic uncertainties, and interpolating. The coloured bands around these lines show the random uncertainty, rescaled as  $\sigma/5$  to keep with the axis scale. Because the random uncertainties and the corrections to the observations are generally very large in comparison to the actual change, scaling the axes is difficult. Note that a consistent colour scheme for the data sources is shown, but not all contribute to every figure.

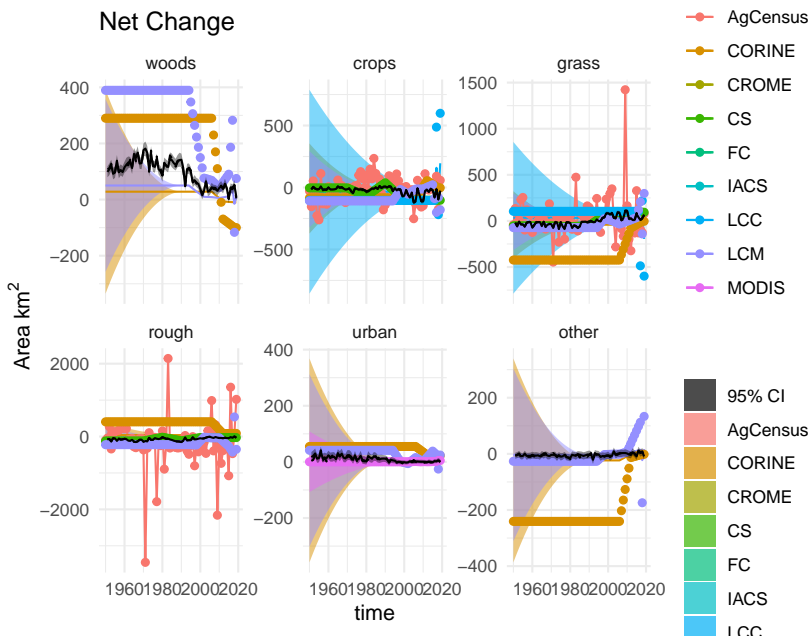


Figure 7.4: Time series of the net change in area occupied by each land use ( $D$ ) from 1950 to 2020, showing the observations and posterior distribution of estimates. The grey shaded band shows the 2.5 and 97.5 percentiles of the posterior distribution. The maximum *a posteriori* estimate is shown as the solid black line within this. Observations from the different data sources are shown as coloured circles. The coloured solid lines show the corrected observations after accounting for systematic uncertainties, and interpolating. The coloured bands around these lines show the random uncertainty, rescaled as  $\sigma/5$  to keep with the axis scale. Because the random uncertainties and the corrections to the observations are generally very large in comparison to the actual change, scaling the axes is difficult. Note that a consistent colour scheme for the data sources is shown, but not all contribute to every figure.

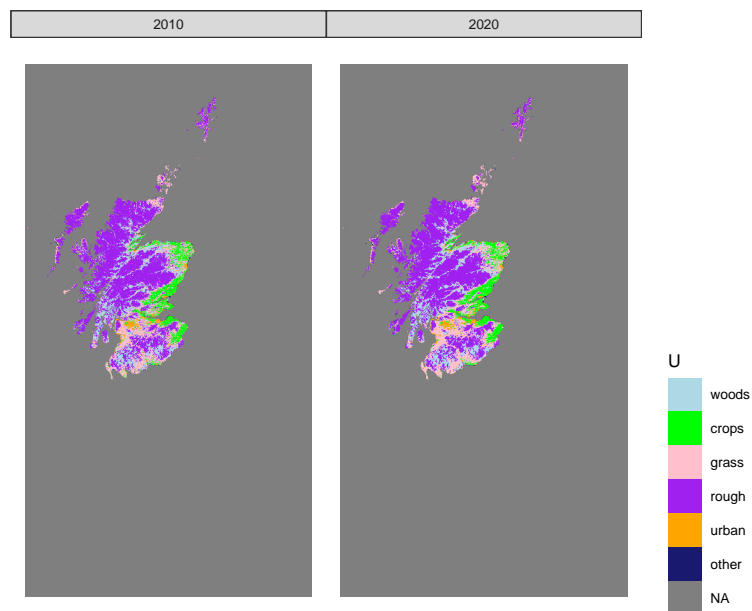


Figure 7.5: Estimated state of land-use in 2010 and 2020 in one realisation of  $U$  from the maximum *a posteriori* estimate of  $B$ .

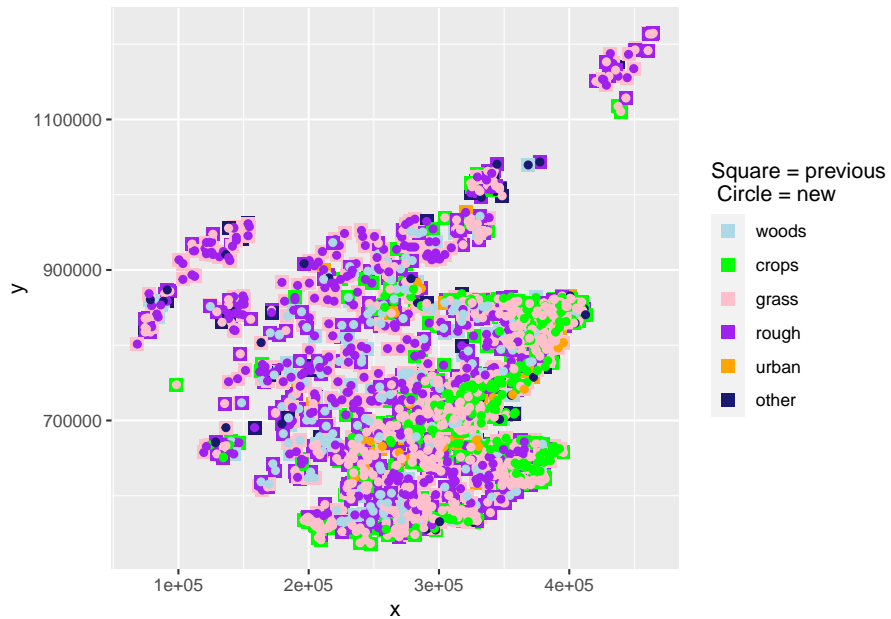


Figure 7.6: The spatial distribution of land-use change between 2010 and 2020 in one realisation of  $U$  from the maximum *a posteriori* estimate of  $B$ . At each location where land use has changed, the use in 2010 is shown as a coloured square, and the use in 2020 is shown as a coloured circle within this

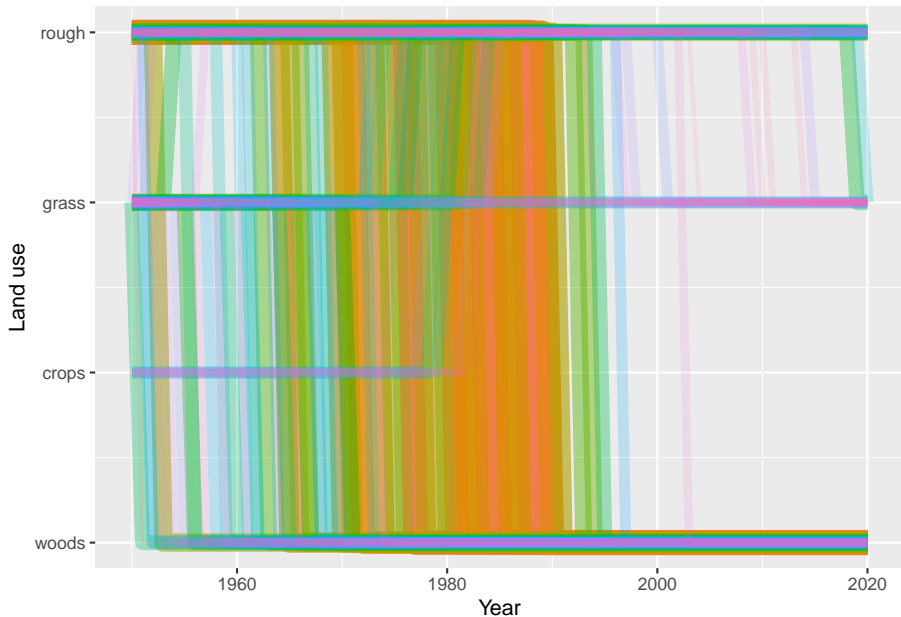


Figure 7.7: Trajectories of the 100 land-use vectors in the posterior  $U$  with the largest areas (excluding the six vectors which show no change). Each vector of land use is shown in a different colour, varied arbitrarily to differentiate different vectors. Line thickness and opacity are proportional to the total area occupied by each vector, so that the dominant vectors are the most visually obvious.

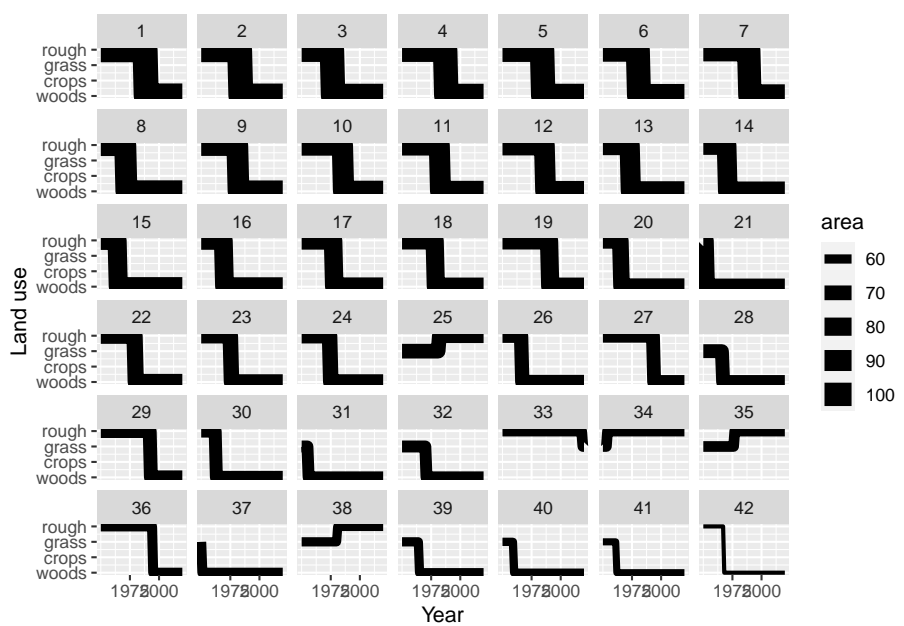


Figure 7.8: Trajectories of the 42 land-use vectors in the posterior  $U$  with the largest areas (excluding the six vectors which show no change). Line thickness is proportional to the total area occupied by each vector.

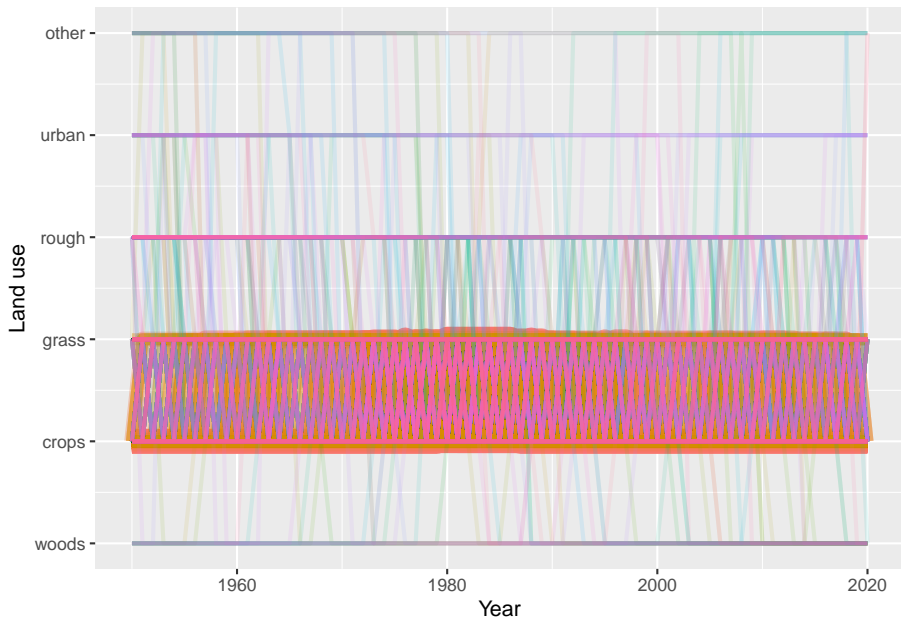


Figure 7.9: Trajectories of the land-use vectors in the posterior  $U$  which involve rotational change between crop and grassland (i.e. those which include either (i) transitions from crop to grass and then subsequently from grass to crop, or (ii) transitions from grass to crop and then subsequently from crop to grass). Each vector of land use is shown in a different colour, varied arbitrarily to differentiate different vectors. Line thickness and opacity are proportional to the total area occupied by each vector, so that the dominant vectors are the most visually obvious.

## **Chapter 8**

### **Results: Wales**

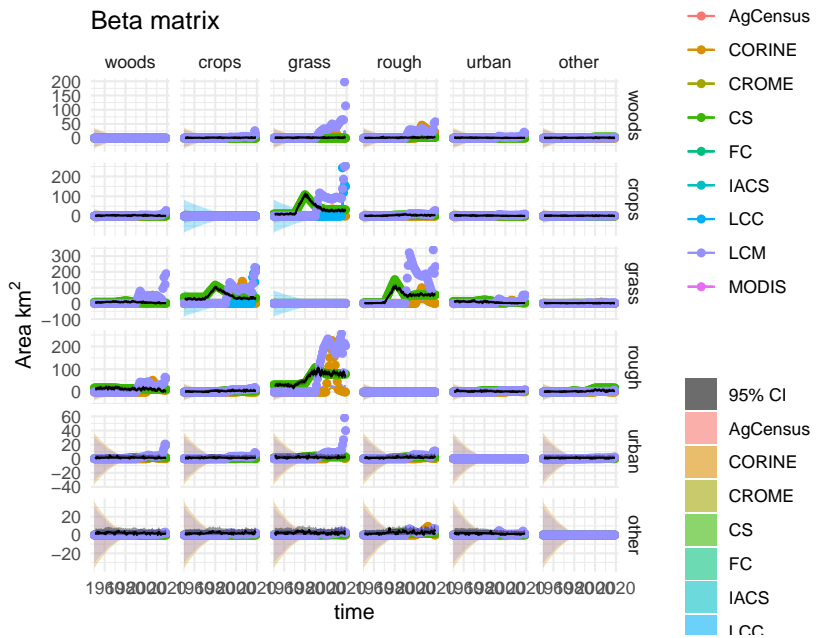


Figure 8.1: Observations and posterior distribution of the transition matrix  $\mathbf{B}$ , representing the gross area changing from the land use in each row to the land use in each column each year from 1950 to 2020. The grey shaded band shows the 2.5 and 97.5 percentiles of the posterior distribution. The maximum *a posteriori* estimate is shown as the solid black line within this. Observations from the different data sources are shown as coloured circles. The coloured solid lines show the corrected observations after accounting for systematic uncertainties, and interpolating. The coloured bands around these lines show the random uncertainty, rescaled as  $\sigma/5$  to keep with the axis scale. Because the random uncertainties and the corrections to the observations are generally very large in comparison to the actual change, scaling the axes is difficult. Note that a consistent colour scheme for the data sources is shown, but not all contribute to every figure.

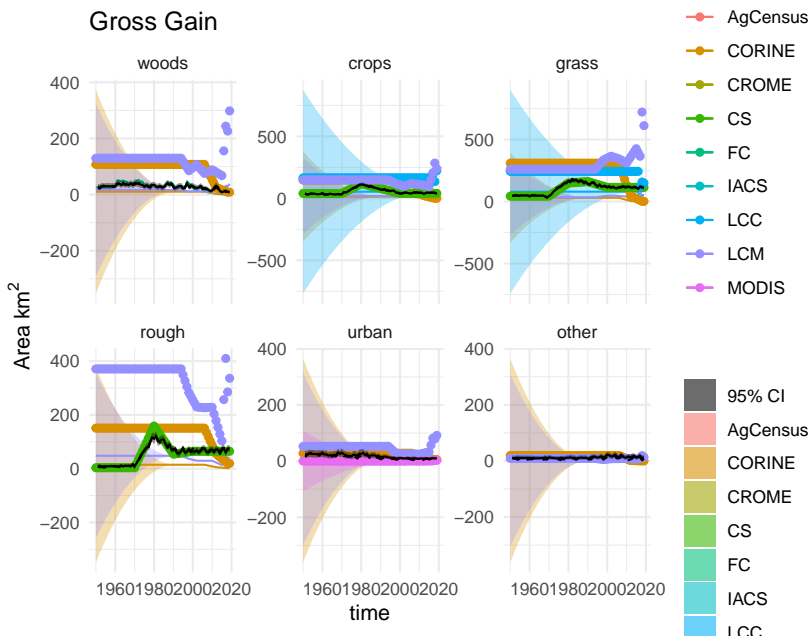


Figure 8.2: Observations and posterior distribution of the gross gain in area of each land use  $\mathbf{G}$  from 1950 to 2020. The grey shaded band shows the 2.5 and 97.5 percentiles of the posterior distribution. The maximum *a posteriori* estimate is shown as the solid black line within this. Observations from the different data sources are shown as coloured circles. The coloured solid lines show the corrected observations after accounting for systematic uncertainties, and interpolating. The coloured bands around these lines show the random uncertainty, rescaled as  $\sigma/5$  to keep with the axis scale. Because the random uncertainties and the corrections to the observations are generally very large in comparison to the actual change, scaling the axes is difficult. Note that a consistent colour scheme for the data sources is shown, but not all contribute to every figure.

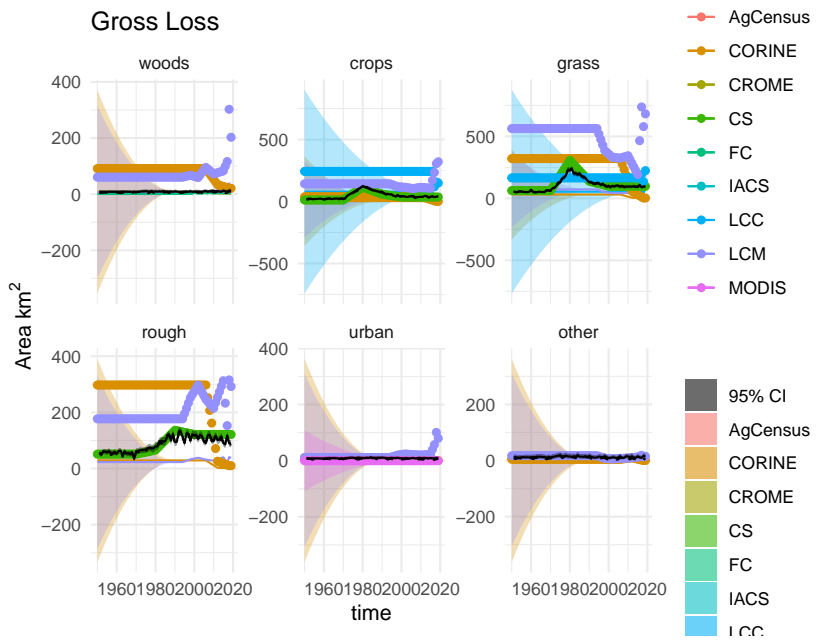


Figure 8.3: Observations and posterior distribution of the gross loss of area from each land use  $\mathbf{L}$  from 1950 to 2020. The grey shaded band shows the 2.5 and 97.5 percentiles of the posterior distribution. The maximum *a posteriori* estimate is shown as the solid black line within this. Observations from the different data sources are shown as coloured circles. The coloured solid lines show the corrected observations after accounting for systematic uncertainties, and interpolating. The coloured bands around these lines show the random uncertainty, rescaled as  $\sigma/5$  to keep with the axis scale. Because the random uncertainties and the corrections to the observations are generally very large in comparison to the actual change, scaling the axes is difficult. Note that a consistent colour scheme for the data sources is shown, but not all contribute to every figure.

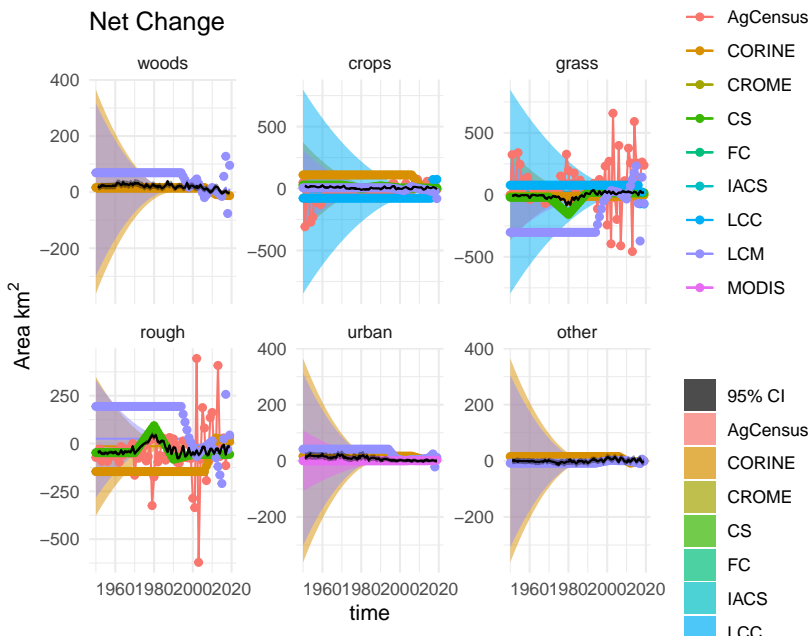


Figure 8.4: Time series of the net change in area occupied by each land use ( $D$ ) from 1950 to 2020, showing the observations and posterior distribution of estimates. The grey shaded band shows the 2.5 and 97.5 percentiles of the posterior distribution. The maximum *a posteriori* estimate is shown as the solid black line within this. Observations from the different data sources are shown as coloured circles. The coloured solid lines show the corrected observations after accounting for systematic uncertainties, and interpolating. The coloured bands around these lines show the random uncertainty, rescaled as  $\sigma/5$  to keep with the axis scale. Because the random uncertainties and the corrections to the observations are generally very large in comparison to the actual change, scaling the axes is difficult. Note that a consistent colour scheme for the data sources is shown, but not all contribute to every figure.

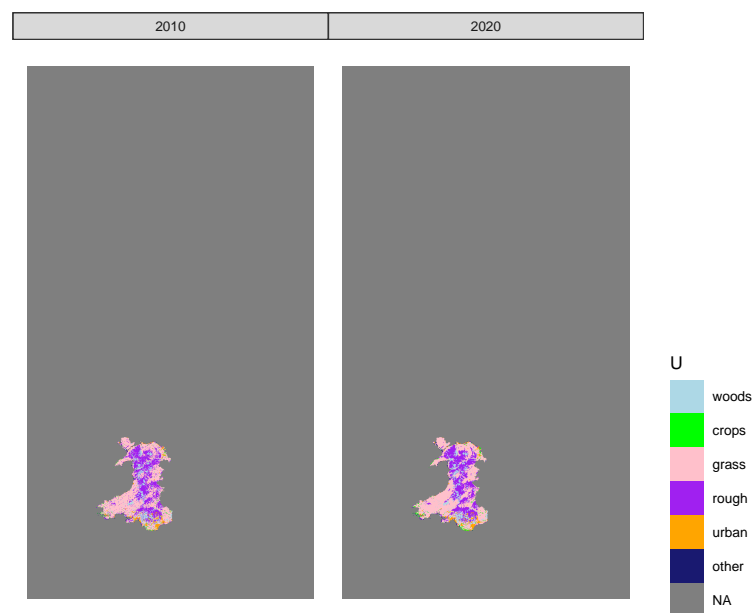
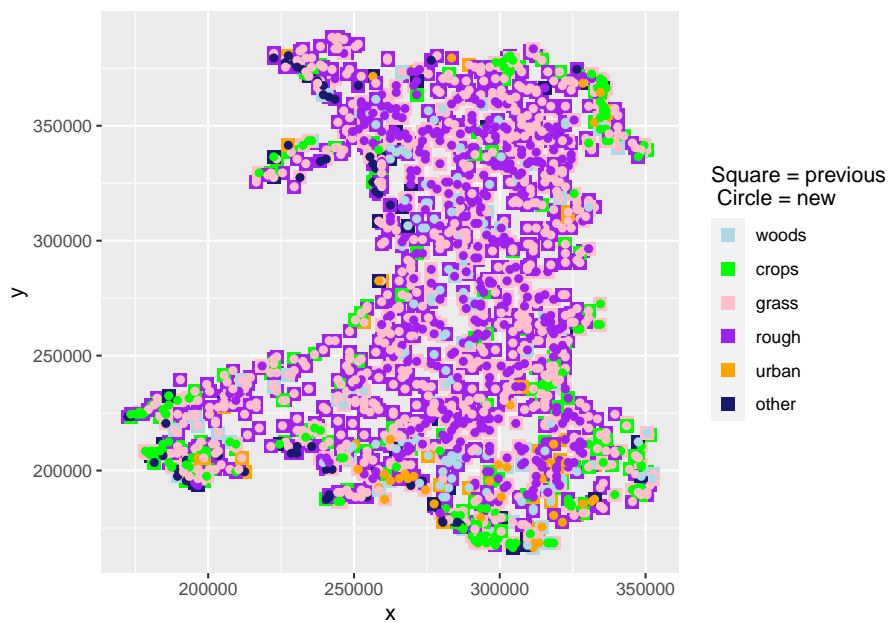


Figure 8.5: Estimated state of land-use in 2010 and 2020 in one realisation of  $U$  from the maximum *a posteriori* estimate of  $B$ .



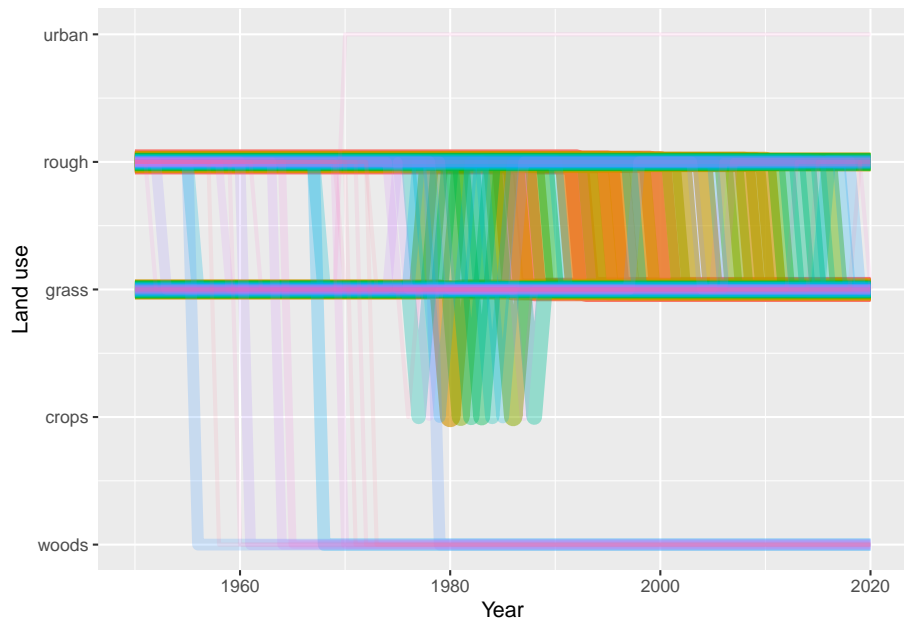


Figure 8.7: Trajectories of the 100 land-use vectors in the posterior  $U$  with the largest areas (excluding the six vectors which show no change). Each vector of land use is shown in a different colour, varied arbitrarily to differentiate different vectors. Line thickness and opacity are proportional to the total area occupied by each vector, so that the dominant vectors are the most visually obvious.

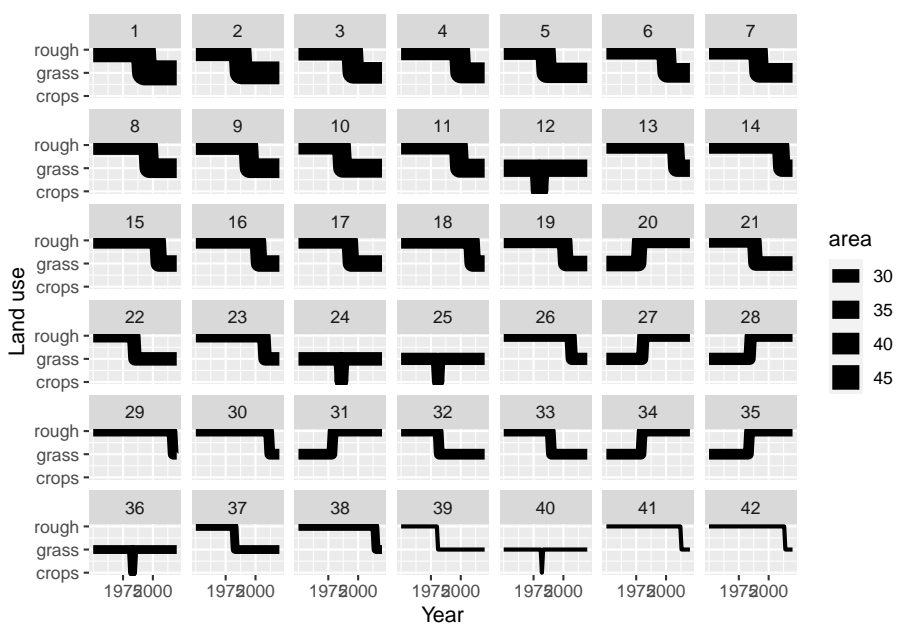


Figure 8.8: Trajectories of the 42 land-use vectors in the posterior  $U$  with the largest areas (excluding the six vectors which show no change). Line thickness is proportional to the total area occupied by each vector.

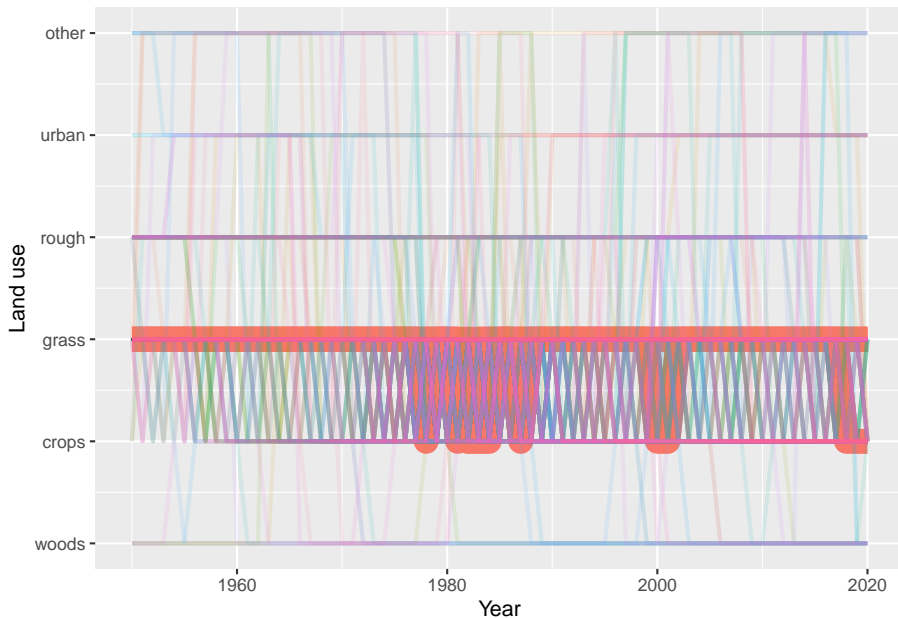


Figure 8.9: Trajectories of the land-use vectors in the posterior  $U$  which involve rotational change between crop and grassland (i.e. those which include either (i) transitions from crop to grass and then subsequently from grass to crop, or (ii) transitions from grass to crop and then subsequently from crop to grass). Each vector of land use is shown in a different colour, varied arbitrarily to differentiate different vectors. Line thickness and opacity are proportional to the total area occupied by each vector, so that the dominant vectors are the most visually obvious.

## **Chapter 9**

# **Results: Northern Ireland**

Levy, P., M. van Oijen, G. Buys, and S. Tomlinson. 2018. “Estimation of Gross Land-Use Change and Its Uncertainty Using a Bayesian Data Assimilation Approach.” *Biogeosciences* 15 (5): 1497–1513. <https://doi.org/10.5194/bg-15-1497-2018>.

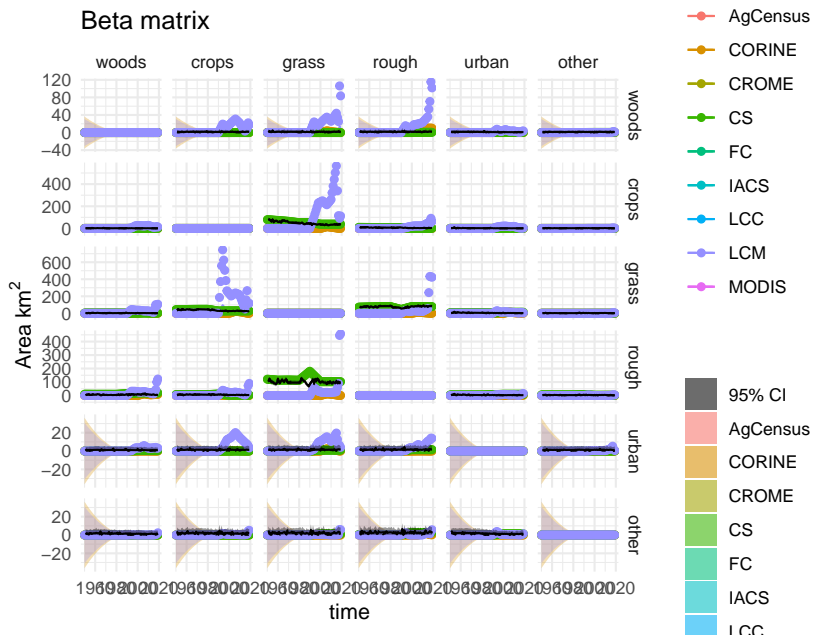


Figure 9.1: Observations and posterior distribution of the transition matrix  $\mathbf{B}$ , representing the gross area changing from the land use in each row to the land use in each column each year from 1950 to 2020. The grey shaded band shows the 2.5 and 97.5 percentiles of the posterior distribution. The maximum *a posteriori* estimate is shown as the solid black line within this. Observations from the different data sources are shown as coloured circles. The coloured solid lines show the corrected observations after accounting for systematic uncertainties, and interpolating. The coloured bands around these lines show the random uncertainty, rescaled as  $\sigma/5$  to keep with the axis scale. Because the random uncertainties and the corrections to the observations are generally very large in comparison to the actual change, scaling the axes is difficult. Note that a consistent colour scheme for the data sources is shown, but not all contribute to every figure.

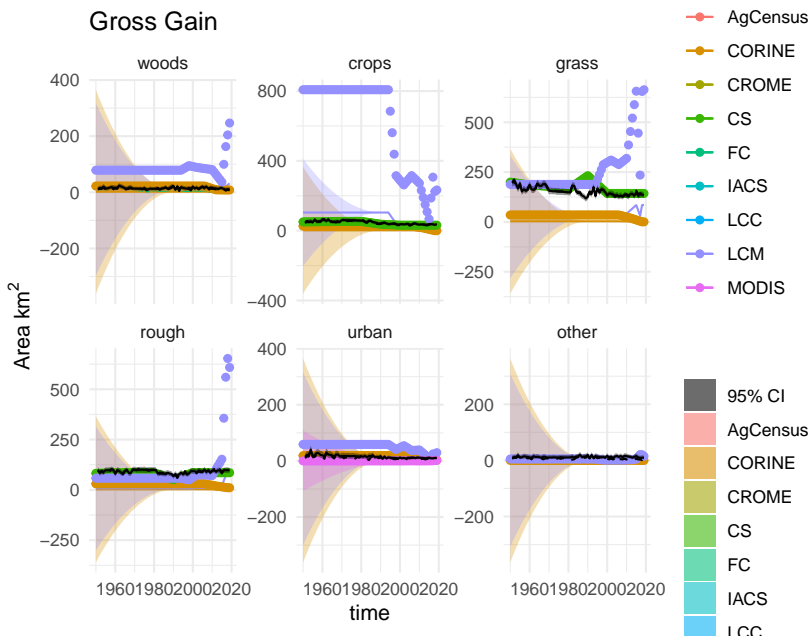


Figure 9.2: Observations and posterior distribution of the gross gain in area of each land use  $\mathbf{G}$  from 1950 to 2020. The grey shaded band shows the 2.5 and 97.5 percentiles of the posterior distribution. The maximum *a posteriori* estimate is shown as the solid black line within this. Observations from the different data sources are shown as coloured circles. The coloured solid lines show the corrected observations after accounting for systematic uncertainties, and interpolating. The coloured bands around these lines show the random uncertainty, rescaled as  $\sigma/5$  to keep with the axis scale. Because the random uncertainties and the corrections to the observations are generally very large in comparison to the actual change, scaling the axes is difficult. Note that a consistent colour scheme for the data sources is shown, but not all contribute to every figure.

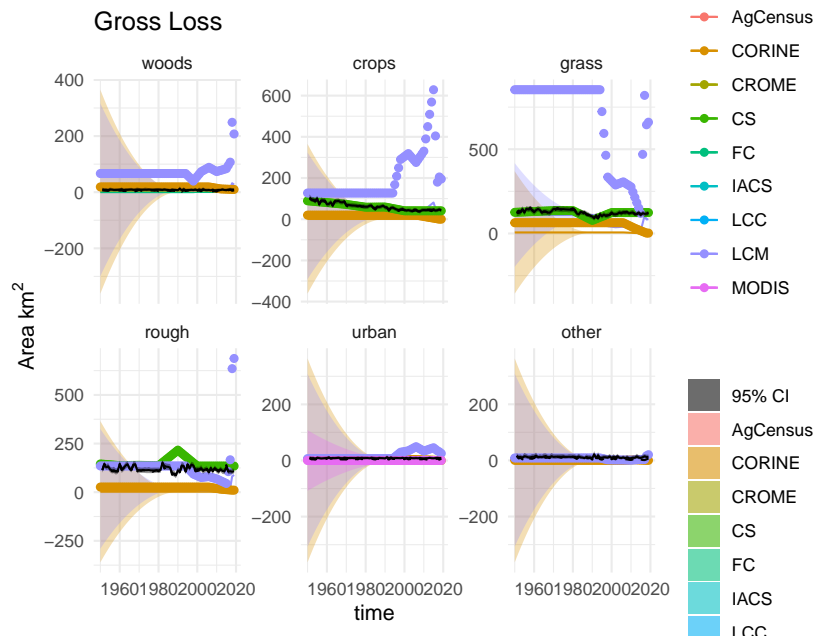


Figure 9.3: Observations and posterior distribution of the gross loss of area from each land use  $\mathbf{L}$  from 1950 to 2020. The grey shaded band shows the 2.5 and 97.5 percentiles of the posterior distribution. The maximum *a posteriori* estimate is shown as the solid black line within this. Observations from the different data sources are shown as coloured circles. The coloured solid lines show the corrected observations after accounting for systematic uncertainties, and interpolating. The coloured bands around these lines show the random uncertainty, rescaled as  $\sigma/5$  to keep with the axis scale. Because the random uncertainties and the corrections to the observations are generally very large in comparison to the actual change, scaling the axes is difficult. Note that a consistent colour scheme for the data sources is shown, but not all contribute to every figure.

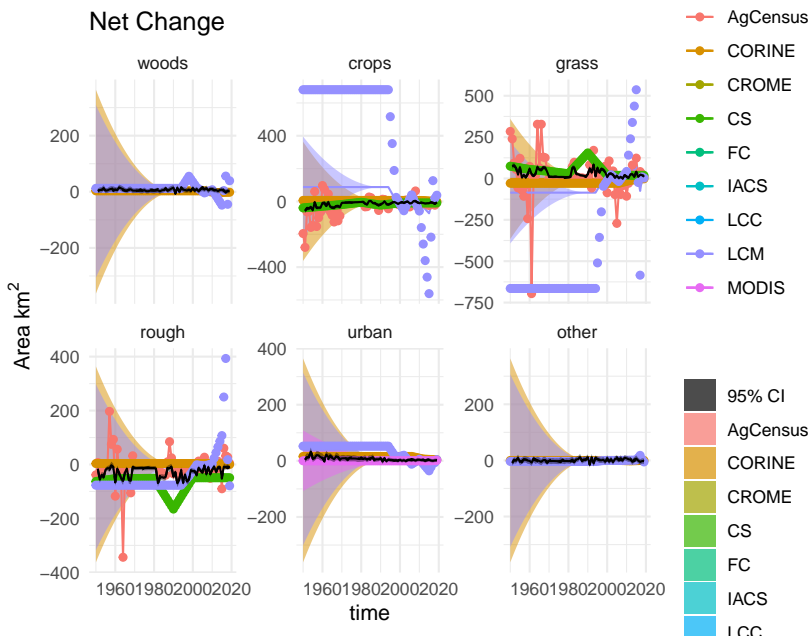


Figure 9.4: Time series of the net change in area occupied by each land use ( $D$ ) from 1950 to 2020, showing the observations and posterior distribution of estimates. The grey shaded band shows the 2.5 and 97.5 percentiles of the posterior distribution. The maximum *a posteriori* estimate is shown as the solid black line within this. Observations from the different data sources are shown as coloured circles. The coloured solid lines show the corrected observations after accounting for systematic uncertainties, and interpolating. The coloured bands around these lines show the random uncertainty, rescaled as  $\sigma/5$  to keep with the axis scale. Because the random uncertainties and the corrections to the observations are generally very large in comparison to the actual change, scaling the axes is difficult. Note that a consistent colour scheme for the data sources is shown, but not all contribute to every figure.

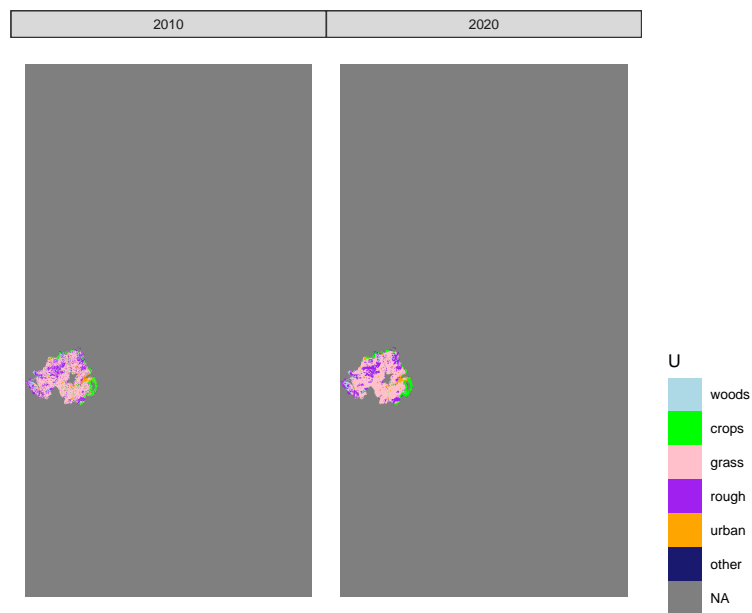
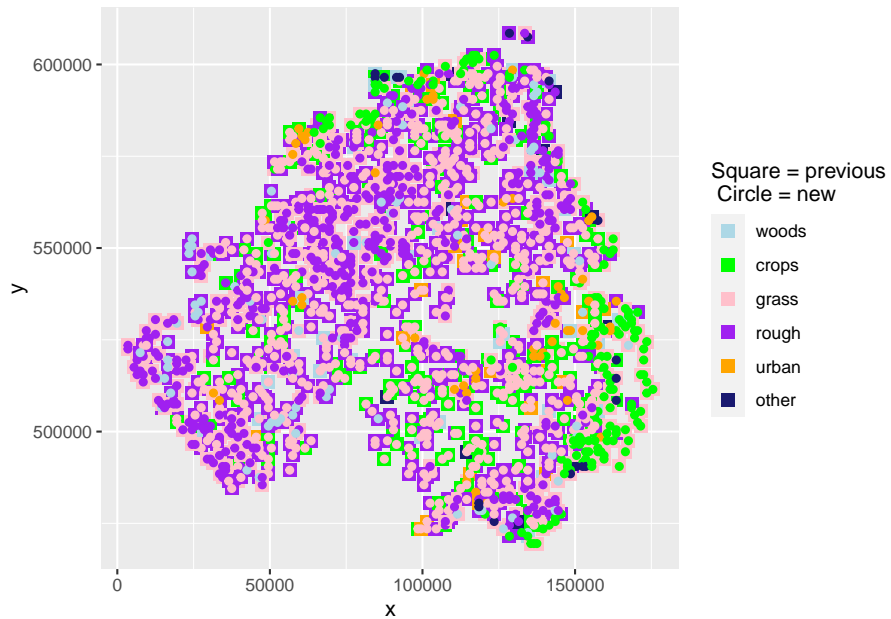


Figure 9.5: Estimated state of land-use in 2010 and 2020 in one realisation of  $U$  from the maximum *a posteriori* estimate of  $B$ .



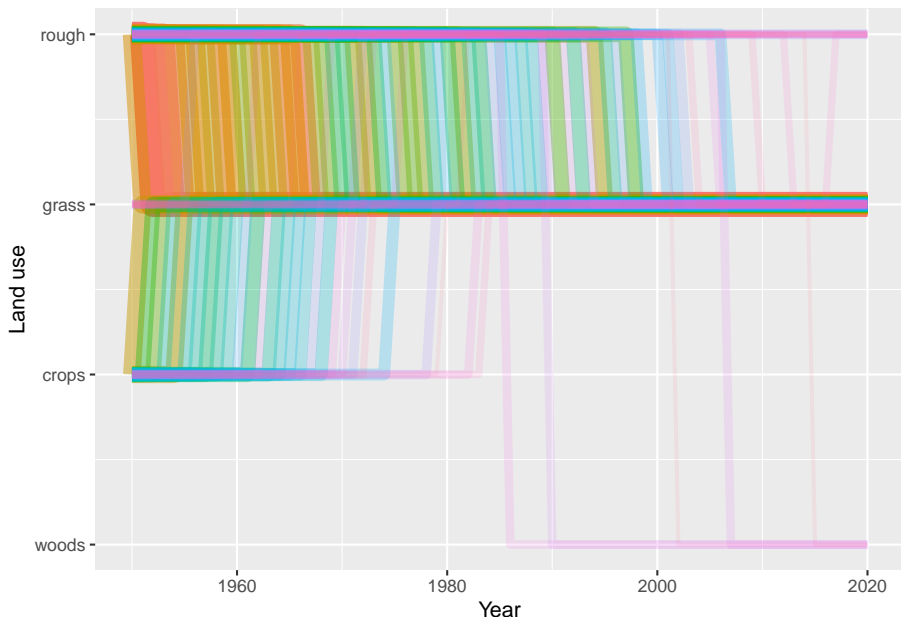


Figure 9.7: Trajectories of the 100 land-use vectors in the posterior  $U$  with the largest areas (excluding the six vectors which show no change). Each vector of land use is shown in a different colour, varied arbitrarily to differentiate different vectors. Line thickness and opacity are proportional to the total area occupied by each vector, so that the dominant vectors are the most visually obvious.

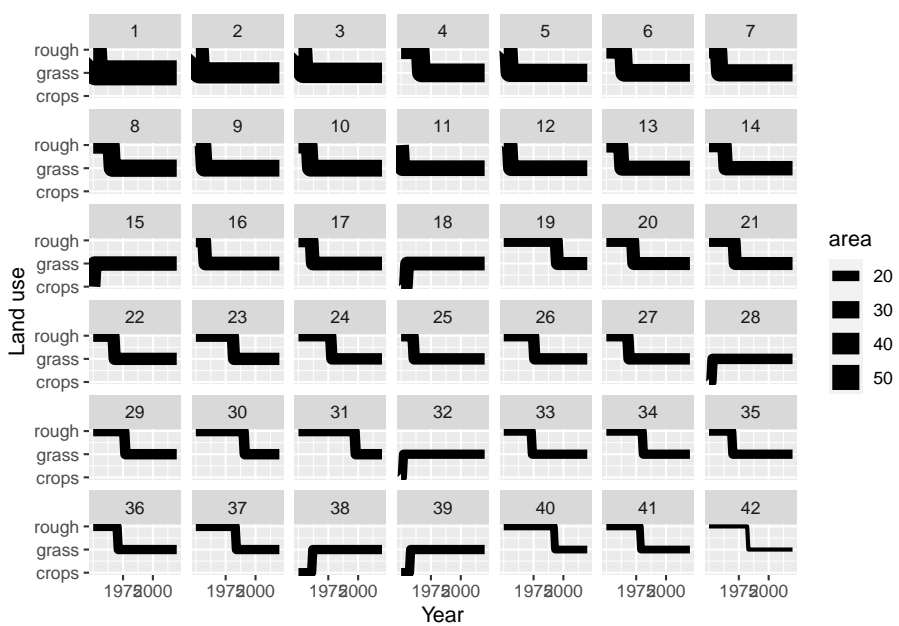


Figure 9.8: Trajectories of the 42 land-use vectors in the posterior  $U$  with the largest areas (excluding the six vectors which show no change). Line thickness is proportional to the total area occupied by each vector.

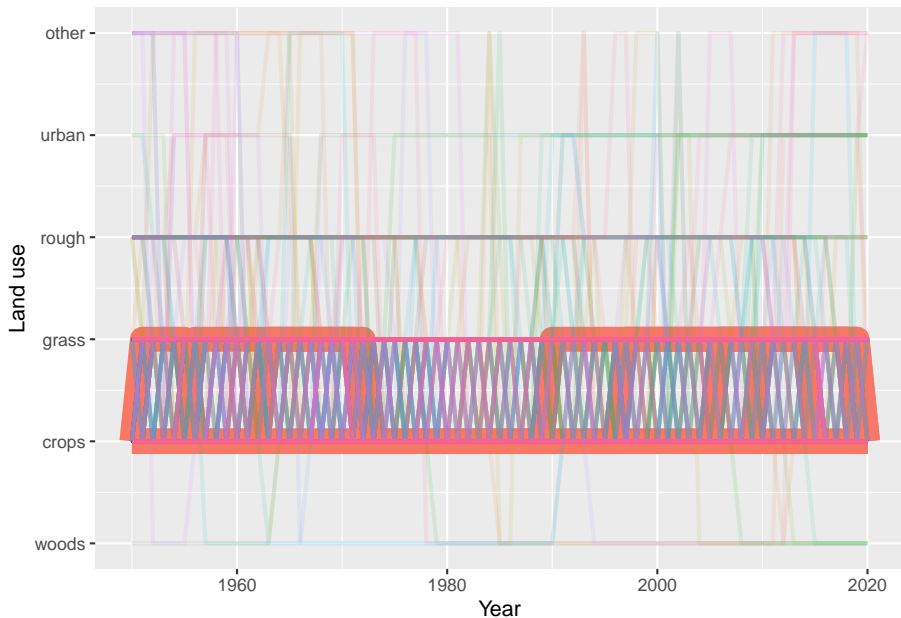


Figure 9.9: Trajectories of the land-use vectors in the posterior  $U$  which involve rotational change between crop and grassland (i.e. those which include either (i) transitions from crop to grass and then subsequently from grass to crop, or (ii) transitions from grass to crop and then subsequently from crop to grass). Each vector of land use is shown in a different colour, varied arbitrarily to differentiate different vectors. Line thickness and opacity are proportional to the total area occupied by each vector, so that the dominant vectors are the most visually obvious.